

REPUBLIC OF TURKEY
YILDIZ TECHNICAL UNIVERSITY
GRADUATE SCHOOL OF NATURAL AND APPLIED SCIENCES

**EVALUATION OF VARIABLE PITCH AND FIXED PITCH
PROPELLER EFFECTS ON A DESIGNED TEST BENCH**

Mehmet ŞANLITÜRK

MASTER OF SCIENCE THESIS
Department of Mechanical Engineering
Machine Theory and Control Program

Advisor
Asst. Prof. Meral BAYRAKTAR, PhD

October, 2019

REPUBLIC OF TURKEY
YILDIZ TECHNICAL UNIVERSITY
GRADUATE SCHOOL OF NATURAL AND APPLIED SCIENCES

**EVALUATION OF VARIABLE PITCH AND FIXED PITCH PROPELLER
EFFECTS ON A DESIGNED TEST BENCH**

A thesis submitted by Mehmet ŞANLITÜRK in partial fulfillment of the requirements for the degree of MASTER OF SCIENCE is approved by the committee on 16.10.2019 in Department of Mechanical Engineering, Mechanical Engineering Machine Theory and Control Program.

Asst. Prof. Meral BAYRAKTAR, PhD

Yıldız Technical University

Advisor

Approved by the Examining Committee

Asst. Prof. Meral BAYRAKTAR, PhD, Advisor

Yıldız Technical University

Asst. Prof. Alpay ORAL, PhD, Member

Yıldız Technical University

Assoc. Prof. Yener TAŞKIN, PhD, Member

İstanbul University - Cerrahpaşa

I hereby declare that I have obtained the required legal permissions during data collection and exploitation procedures, that I have made the in-text citations and cited the references properly, that I haven't falsified and/or fabricated research data and results of the study and that I have abided by the principles of the scientific research and ethics during my Thesis Study under the title Evaluation of Variable Pitch and Fixed Pitch Propeller Effects on a Designed Test Bench supervised by my supervisor, Asst. Prof. Meral BAYRAKTAR. In the case of a discovery of false statement, I am to acknowledge any legal consequence.

Mehmet ŞANLITÜRK

Signature

ACKNOWLEDGEMENTS

First of all, I would like to express my sincere gratitude to my advisor Asst. Prof. Meral Bayraktar for her valuable guidance, support and advice throughout my research.

I would like to express my special appreciation to Dr. Ahmet Kırılı, and all other academic staff of YTU for their instructive and rewarding lectures.

Special thanks to my dear desk-friends Murat İbrahimağaoğlu, his wife İpek İbrahimağaoğlu and Burak Turan for their support and sincere friendship.

I would also like to thank all my friends especially Orcun who supported me and made me feel happy especially during the difficult times.

Finally, I am also grateful to my lovely family, I would like to specially thank my father and mother for their invaluable support and love especially at hard times of my life.

Mehmet ŞANLITÜRK

TABLE OF CONTENTS

LIST OF SYMBOLS	vii
LIST OF ABBREVIATIONS	ix
LIST OF FIGURES	x
LIST OF TABLES	xi
ABSTRACT	xii
ÖZET	xiv
1 Introduction	1
1.1 Literature Review.....	2
1.2 Objective of the Thesis	5
1.3 Hypothesis.....	5
2 Unmanned Aerial Vehicles with Four Rotors	6
2.1 Basic Concept.....	7
2.2 Dynamic Model of Quadrotor	9
2.3 Mathematical Model of Motor	10
2.4 Aerodynamic Analysis of Propeller	11
2.4.1 Blade Element Theory	12
3 Test Bench System	17
3.1 Objective of Experiment	17
3.2 Test Bench Main Frame Strain Analysis	18
3.3 DC Motor	20
3.4 Propeller Model.....	22
3.5 Electronic Speed Controller.....	25
3.6 Hall Effect Sensor.....	27
3.7 Force Sensor	28
3.8 Test Bench Model	29
3.9 Findings of Lift Force Measure.....	31

4	Controller Design	34
4.1	Motor Model Control.....	34
4.2	Stability of Motor Model	35
4.3	PID Model	36
5	Conclusion	40
5.1	Conclusion.....	40
5.2	Future Work	41
	References	42
	Publications from the thesis	44
	Appendix	45

LIST OF SYMBOLS

α	Angle of Attack
θ	Roll Angle
ϕ	Pitch Angle
ψ	Yaw Angle
θ_p	Pitch Angle of Propeller
A	Frontal Area of the Propeller
C_L, C_{D0}	Lift Coefficient at Minimum Drag
C_{D2l}	Parasitic Drag Coefficient
C_{D2u}	Lift Coefficient Quadratic Parameter
C_{Di}	Lift-Induced Drag Coefficient
C_{L0}	Lift Coefficient at Zero Pitch
$C_{L\alpha}$	Lift Coefficient
C_{D0}	Linear fit of C_L to α
C_{Lmax}	Maximum Lift Coefficient
C_{Lmin}	Minimum Lift Coefficient
F_i	Thrust Force
F_L	Lift Force
F_D	Drag Force
I_R	The Inertia Moment
k_g	Motor Gain
k_m	Torque Factor
k_n	Thrust Factor
K_i	Integral Gain

K_d	Derivative Gain
K_p	Proportional Gain
M	Moment Vector
N_b	Blade Number
R	Propeller Radius
R_e	Reynolds Number
RE_{exp}	Reynolds Number Adjusting Factor
RE_{ref}	Reynolds Number for Drag Calculations
T_i	Torque
U_1	Total Force Generated by Four Propeller
U_2	Differential Moment between Right and Left Propeller
U_3	Differential Moment between Front and Rear Propeller
U_4	Net Torque
V	Airflow velocity
v	Propeller Linear Velocity
v_i	Induced Velocity
ω_i	Motor Speed
ρ	Air Density
ω, Ω	Angular Velocity
λ	Inflow Ratio

LIST OF ABBREVIATIONS

BET	Blade Element Theory
DC	Direct Current
ESC	Electronic Speed Controller
FSR	Force Sensitive Resistor
NACA	National Advisory Committee for Aeronautics
NASA	National Aeronautics and Space Administration
PCB	Printed Circuit Board
PID	Proportional Integral Derivative
RC	Radio Controlled
RPM	Revolutions Per Minutes
TF	Transfer Function
UAV	Unmanned Aerial Vehicles

LIST OF FIGURES

Figure 2.1	The Various Direction of Movement of the Quadrotor [18]	8
Figure 2.2	Force and Torque Generated by Each Propeller and Rotor Configuration	9
Figure 2.3	Forces on the Airfoil [20]	11
Figure 2.4	Drawing of airfoil [21]	13
Figure 2.5	Airfoil cross section area and forces [21]	13
Figure 3.1	Concept Design of the Thrust Measurement Test Bench [23]	17
Figure 3.2	Material Property of Plexiglas G [®]	18
Figure 3.3	The Boundary Conditions of Test Bench System and the Force	19
Figure 3.4	Strain Analysis Result	19
Figure 3.5	Brushless DC motor	21
Figure 3.6	Propeller Pitch Motion [23]	23
Figure 3.7	Propeller Pitch	23
Figure 3.8	The Variable-Pitch Mechanism and Corresponding Propellers	24
Figure 3.9	Electronic Speed Controller	26
Figure 3.10	Hall Effect Sensor and Magnets	27
Figure 3.11	Force Sensitive Resistor Sensor	28
Figure 3.12	The Resistance/The Force Graph of FSR [25]	28
Figure 3.13	Test Bench	30
Figure 3.14	Schematic Representation of Test Apparatus	29
Figure 3.15	Lift Force – Pitch Angle – Rotational Speed (rpm) Graph	32
Figure 3.16	Lift Force – Rotational Speed (rpm) Graph (Pitch Angle is constant and equal 0°)	33
Figure 4.1	Motor Model Root Locus	35
Figure 4.2	Step Response of Motor Model	36
Figure 4.3	Typical PID Structure	37
Figure 4.4	General Overview of Both Model	38
Figure 4.5	Altitude Trajectory	39

LIST OF TABLES

Table 2.1	Advantages and Disadvantages of Quadrotor.....	6
Table 2.2	Fixed-Pitch and Variable-Pitch Propellers: Advantages and Disadvantages [17]	7
Table 3.1	Technical Specifications of Brushless DC Motor	21
Table 3.2	Technical Specifications of Variable Pitch Unit	25
Table 3.3	Propeller Aerodynamic Coefficients According to NACA.....	25
Table 3.4	Types of Equipment of Test Bench.....	30
Table 3.5	Lifting Forces Caused by Angle and Speed Changes.....	31
Table 4.1	Ziegler-Nichols Method	38
Table 4.2	Altitude Control with Ziegler-Nichols Method	38

Evaluation of Variable Pitch and Fixed Pitch Propeller Effects on a Designed Test Bench

Mehmet ŞANLITÜRK

Department of Mechanical Engineering

Machine Theory and Control

Advisor: Asst. Prof. Meral BAYRAKTAR, PhD

Multi-rotor unmanned aerial vehicles (UAVs) have been trending among academics and professionals. It has a wide scope of use in industries like cargo transportation, measurement, mapping, video and photo shooting, search and rescue, agriculture, and construction. Despite its advantages in movement and control, it gives too little hover time. A great deal of quadrotor or multirotor propeller designs have a fixed-pitch propeller which is mechanically simple. In addition, it provides excellent maneuverability, survivability and controllability. Variable-pitch propellers are used in many practices such as ships, aircrafts, helicopters and recently quadrotor applications.

In this study, it is aimed to find the lift force generated on the rotor by changing the angles of the propeller at the constant speed and design a prototype with optimized PID with coefficients. A pre-model was tested to determine the generated lift force and simulated the altitude trajectory of quadrotors. The simulation results compared with the controller using PID coefficients.

The measurements of this experimental testing support the potential benefits of the variable-pitch propellers. This research shows the difference between fixed and variable pitch angle applications with optimized PID. It is concluded that when compared in terms of altitude trajectory control, it is found that variable-pitch propeller tracks a better trajectory than fixed-pitch propeller.

Key words: Unmanned aerial vehicles (UAVs), variable-pitch propellers, test bench, PID

Değişken ve Sabit Hatveli Pervane Etkilerinin Tasarlanmış Test Düzenegi Üzerinde Karşılaştırılması

Mehmet ŞANLITÜRK

Makine Mühendisliği Bölümü

Yüksek Lisans Tezi

Danışman: Asst. Prof. Meral BAYRAKTAR

Multi-rotorlu insansız hava araçları (İHA) hem akademik alanda hem de uygulama anlamında giderek artan bir eğilim yakalamıştır. Kargo taşımacılığında, ölçüm, haritalama, video ve fotoğraf çekimlerinde, arama-kurtarma, tarım ve inşaat sektöründe vb. alanlarında kullanılmaktadır. Hareket kabiliyeti ve kontrollünün kolay olmasına karşın en büyük dezavantajı hava kalma süresidir.

Bu çalışmada sabit devirde kanat açılarını değiştirerek rotorda oluşan kuvveti bulunmuştur ve buna uygun PID ile çalışan kontrolcü tasarlanmıştır. Test düzeneği oluşturularak rotorun ürettiği kuvvet bulunup buna uygun olarak PID kontrolcü ile simüle edilmiştir. Test düzeneğinden elde edilen kontrolcünün tasarımında kullanılan veriler ile PID katsayıları kullanılarak yapılan kontrolcü arasında karşılaştırılma yapılmıştır. Çalışmanın amacı, sabit ve değişken kanat açıları arasındaki farkı ortaya koymaktır.

Anahtar Kelimeler: İnsansız hava araçları (İHA), değişken hatveli pervane, test düzeneği, PID

Small quadrotor with electric motors and fixed-pitch propellers have gained popularity among academicians and hobbyists recently. Many quadrotor and multirotor designs use a fixed-pitch propeller that is mechanically simple, but variable-pitch propellers are excellent in terms of maneuverability and controllability and present in all modes of transportation such as ships, airplanes, helicopters. They are expected to be used in more sectors shortly, such as commercial and military drones.

According to the Goldman Sachs research, by 2020, market opportunity for drones is estimated to be \$100 billion, helped by increasing demand from military, consumer, commercial and civil government sectors [1]. While drones use in such a large area, it is not possible to ignore the fact that even a small improvement in flight efficiencies of drones will lead to energy savings and an increase in utilization rates in total. Therefore, it is crucial for drones to work with efficiency. The efficiency of the aircraft is determined by the time it floats in the air. Standard drones include motor drives, motors, batteries, and propellers. In order to increase float time, it is also important to focus on the efficiency of each component. However, in this study, different equipment is used as against to standard drone applications, aiming to eliminate the loss of efficiency in the motor by changing of the propeller pitch.

In this study, lift force by a variable-pitch rotor is measured with a test system, to use it in the improvement of flight efficiency of drones.

1.1 Literature Review

Brushless DC electric motors, telecommunication systems, high energy-capacity-to-weight batteries, light material, and flight controllers have led to the popularization of UAVs for civilian, commercial and recreational applications [2].

Attempts have also been made to enhance the agility of multi-copters by changing their mechanical design. In particular, variable-pitch propellers have been given to allow multi-copters to fly in ways that conventional quadcopters cannot [3].

Variable-pitch quadrotors have been tested for a while. The HoverBot - an example - performed well in most cases but failed in autonomous flight. [4].

By minimizing the system energy for a command thrust value, the optimizer calculates the optimum pitch angle of a variable pitch propeller. This algorithm is tested on a DC motor that drives a variable-pitch propeller; the DC motor and variable-pitch propeller's experimental hardware configuration is described [5].

The mathematical model of quad-rotor was determined by movement and rotation equations according to Newton's laws. Besides, the PID controller was designed and tested in the simulation to keep the quadrotor's height constant [6].

The mechanical design and autonomous control of a conventional engine (gasoline) variable-pitch quadcopter prototype are developed. The objective of the prototype is to extend the flight endurance of conventional quadrotor, which is almost entirely powered by the battery. End of the thesis, the prototype accomplishes this objective by exploiting the high energy density of fossil fuels [7].

"X4 Flyer" model is examined as a four-rotor air robot that can perform vertical take-off and landing in indoor applications. The model of the system is given, and the pilotage control design is emphasized. Modeling is done with MATLAB-Simulink. Tests have shown that the internal loop controller is operating correctly [8].

A mechanism for testing control algorithms for unmanned aerial vehicles is contemplated. It is determined that the modeling is consistent with the tests performed in the setup. Due to the direct connection of the vehicle to the test

apparatus, which has six degrees of freedom, a measurement of the vehicle's movements cannot be taken. [9]

Computer controlled small scale flying vehicle design and mechanical structure of vehicle are emphasized. As a result of the experiments in the laboratory, it is revealed that safety is the most essential. Two types of tests are carried out in the test set up as a two-propeller system. In the first test, vertical height stability of drone is checked with PID. In this test, it is found that the cable weights had great effects on the system as the vehicle's height increased. In the second test, position control is repeated with different control parameters. The lack of this work is that the vehicle has not been fully tested since it has not been operated under real thrust forces [10].

Modeling and control have been studied for 4-rotor UAVs. A widely used dynamic model has been improved and a hybrid controller has been obtained with various combinations of PID-based conventional controller. The control of the aircraft was discussed in 3 stages. The height, the position on the x, y axes and finally yaw motion were checked, respectively, and a different controller was designed for each step [11].

Proportional to the increase in the size of the quadrotors, it becomes harder to control the motor by means of a change in rotational speed alone. This is due to the fact that larger motors have larger inertias and the torque needed to correct the rotational velocity of the motor surpass the motor's capacity, therefore, it doesn't allow for a control system to react as quickly. So for larger motors, the variable-pitch blades only act as a stabilizer [12].

Some hobbyists have been working on RC variable-pitch quadrotors quite a while. Although there's no work published yet, a model displayed features such as autonomous take-off upside-down flights and flips [13] [14].

The article was about the control and experimental model of a quadrotor with variable pitch propeller, the studies are grouped under three main sections. These sections are that theoretic development and evaluation of new models for variable pitch propellers, optimization of the variable pitch - propulsion configurations and

calculation and evaluation of the performance of variable pitch propellers. It demonstrated that variable pitch control improves efficiency for quadrotors. Variable-pitch control is almost twice as fast as the fixed-pitch model control [15].

In the article about the design and flight tests of a quadrotor with pitch variable, it was mentioned that fixed-pitch quadrotors were controlled only by the differential motor speed and the control bandwidth was limited to the rotational inertia of the motors. However, it stated that the control bandwidth would limit the agile maneuvers that a quadrotor can perform, and therefore, the delicate and skilled maneuvers limit the application areas of the quadrotor. Controlling the bandwidth in conventional vehicles was a method of control that becomes even more difficult with the increase of the size of the quadrotor, and since the torque required to change the motor speed rapidly exceeds the capacity of the motor speed, the quadrotor residual speed control becomes uncontrollable by the standard. Controlling the bandwidth in conventional drones was a method of control that becomes even more difficult with the increase of the size of the quadrotor, and since the torque required to change the motor speed rapidly exceeds the capacity of the motor speed, the quadrotor residual speed control becomes uncontrollable. Controlling the bandwidth in conventional drones was a method of control that becomes even more difficult with the increase of the size of the quadrotor, and since the torque required to change the motor speed rapidly exceeds the capacity of the motor speed, the quadrotor speed control no longer becomes uncontrollable. For this reason, it was emphasized that variable pitch propellers may be necessary for large four rotors and also for standard use.

To control the angles of the propellers, 4 pieces digital, high-speed Futaba servos with less than 10 grams were used. It is aimed to keep the motor speed constant under variable load conditions to drive the brushless DC motors in the system by using the Hacker electronic speed controller. With continuous closed-loop motor speed control in the system and providing pitch angle change of servos increase the reliability and stabilization of the vehicle under variable conditions. In the first flight tests in this article, the feasibility of the variable pitch control system was made, and in the course of nominal trajectory monitoring experiments, it proved to better

results well than the standard fixed-pitch quadrotors. In addition, the experiments were repeated with different concepts. The vehicle was tested to be reversed flight by reversing and basic improvements were observed by comparing the current drawn by the fixed-pitch quadrotors. Although the vehicle is still under development, tests show that the performance of the variable pitch quadrotor will be improved compared to fixed-pitch quadrotor [16].

1.2 Objective of the Thesis

This study aims to make an experimental setup for the propeller of the rotor and to improve the UAV in terms of mechanical, mechatronics and control and to bring them to the desired level. The experimental setup provides many possibilities in terms of spatial mobility. This thesis discusses variable-pitch propellers mainly overcome the limitations resulting from fixed-pitch propeller.

It is thought that an experimental setup that offers many possibilities in terms of scope will be very beneficial for UAVs.

According to the aim of the thesis, test bench, hardware, software, and control model have been improved in this period as well as the targeted result has been achieved.

1.3 Hypothesis

This thesis explores how and why variable-pitch propellers outperform fixed-pitch propellers. This experimental setup is promising in advancing spatial mobility.

The method followed by during measurement;

1. The pitch-angle of the propeller is constant while the lift force is generated by changing the motor rotational speed.
2. The motor rotational speed is constant while the lift force is generated by changing the pitch-angle of the propeller.

Unmanned Aerial Vehicles with Four Rotors

Quadrotor is one of the most preferred unmanned aerial vehicles (UAV)s that can fly on its own without an operator. Quadrotor has many advantages in terms of control and easy installation compared to conventional helicopters, but also disadvantages. Directional control and stability are very difficult to achieve due to the non-linearity of their dynamics.

In general, the advantages and disadvantages of quadrotor are shown in Table 2.1.

Table 2.1 Advantages and Disadvantages of Quadrotor

Advantages	Disadvantages
Simple mechanic	High energy consumption
Reduced gyroscopic effects	The payload carrying capacity
Easy setup	Flight endurance, flight range
Variety of using area	Directional control and stability
Autonomous pilot	
Take off and land vertically, hovering, aggressive maneuverability	

To date, generally, the fixed-wing propeller is used in the quadrotors. Moreover, almost whole studies are about the fixed-wing propeller. Because the fixed-wing propeller is easy to implement and control in the quadrotor. Recent studies have been doing about the variable-pitch propellers in quadrotor.

Variable-pitch propellers mostly exceed the limits of the fixed-pitch flight. In addition, reversed thrust is achieved efficiently. The inertia of the motor-propeller combination determines the limit of the fixed-pitch quadrotor control bandwidth.

On the other hand, the speed of the variable-pitch actuation determines the only limit of the variable-pitch quadrotor control bandwidth. Evaluation of both mechanisms; the fixed-pitch and the variable-pitch propellers is shown in Table 2.2.

Table 2.2 Fixed-Pitch and Variable-Pitch Propellers: Advantages and Disadvantages [17]

	Advantages	Disadvantages
Fixed-Pitch Propellers	<ul style="list-style-type: none"> - Simple mechanical set-up - Uncomplicated dynamics - Robust and reliable control - Simple and low-cost design - Require minimum maintenance 	<ul style="list-style-type: none"> - Weak maneuverability due to the control limits
Variable-Pitch Propellers	<ul style="list-style-type: none"> - Effective reversed thrust - Higher control bandwidth - Aerobatic and aggressive maneuverability 	<ul style="list-style-type: none"> - Complicated mechanical set-up - Complexed dynamics - Fragile mechanism - Complicated and high cost design - Require more maintenance

2.1 Basic Concept

The quadrotor is equipped with four propellers driven by four motors positioned in a cross configuration. The front and the rear motors rotate in the counterclockwise direction while the right and the left motors rotate in the clockwise direction. If the gyroscopic effects were neglected when rotors rotate at the same speed, the quadrotor would take off. The thrust generated by each motor must be the same to achieve stable hover condition.

This is an under-actuated vehicle which can only be driven through the control of each rotor thrust. Changing the thrust of specific rotor leads to the three basic attitude changes (pitch, roll, yaw) and altitude control. The quadrotor is capable of vertical take-off and landing, furthermore can be hovered in the air and rotated around their axis.

Figure 2.1 shows the direction of movement of the quadrotor according to the force generated by the propellers and the direction of rotation. The front and rear motors (1 and 3) rotate in the opposite direction of the clock (counterclockwise), the right and left motors (2 and 4) rotate clockwise, while the thick arrows show the fast rotation, the thin arrows indicate the slow rotation.

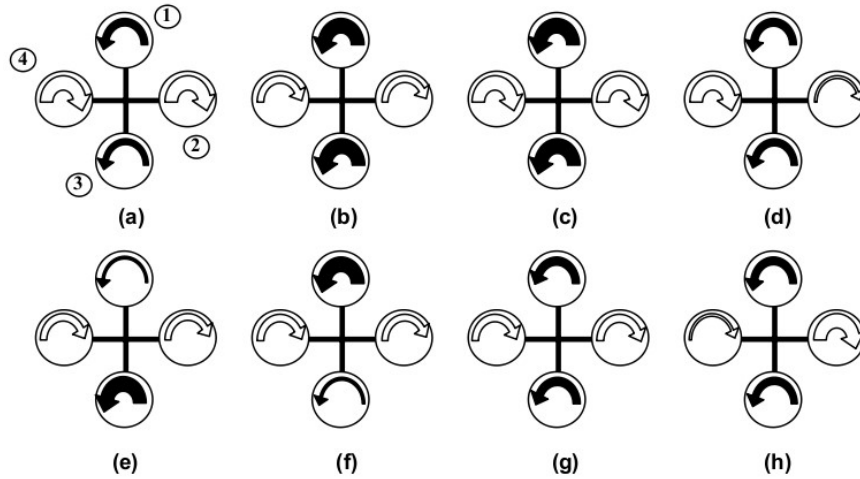


Figure 2.1 The Various Direction of Movement of the Quadrotor [18]

- | | |
|---|---|
| (a) Yaw (counterclockwise direction) | (e) Pitch (counterclockwise direction) |
| (b) Yaw (clockwise direction) | (f) Pitch (clockwise direction) |
| (c) Take-off or take-up | (g) Land or take-down |
| (d) Roll (clockwise direction) | (h) Roll (counterclockwise direction) |

When Figure 2.1 is examined in detail, yaw occurs when the thrust of the mutual rotors is increased. The direction of the yaw is shown in Figure 2.1.a and Figure 2.1.b. It is seen that the yaw is in the direction of the rotor with less angular velocity or less lift force.

When the force of one of the opposing rotor pairs is increased, pitch and roll occur. When the force of the 2nd or 4th rotors is increased, it causes the roll as seen in Figure 2.1.d and Figure 2.1.h. Similarly, when the force of the 1st or 3th rotors is increased, it causes pitch as seen in Figure 2.1.e and Figure 2.1.f.

By increasing speeds of mutual rotor pair in the direction which they rotate is provide take-off motion Figure 2.1.c and by decreasing is provide land motion Figure 2.1.g.

2.2 Dynamic Model of Quadrotor

In this section, the motion of the quadrotor is examined mathematically using Newton-Euler equations. The following equations are used as the model of the quadrotor. The study is experimental and focuses on the control of aircraft.

First, the control inputs U_1, U_2, U_3 and U_4 are defined, and then it is aimed to explain their relation with the dynamics of the motor.

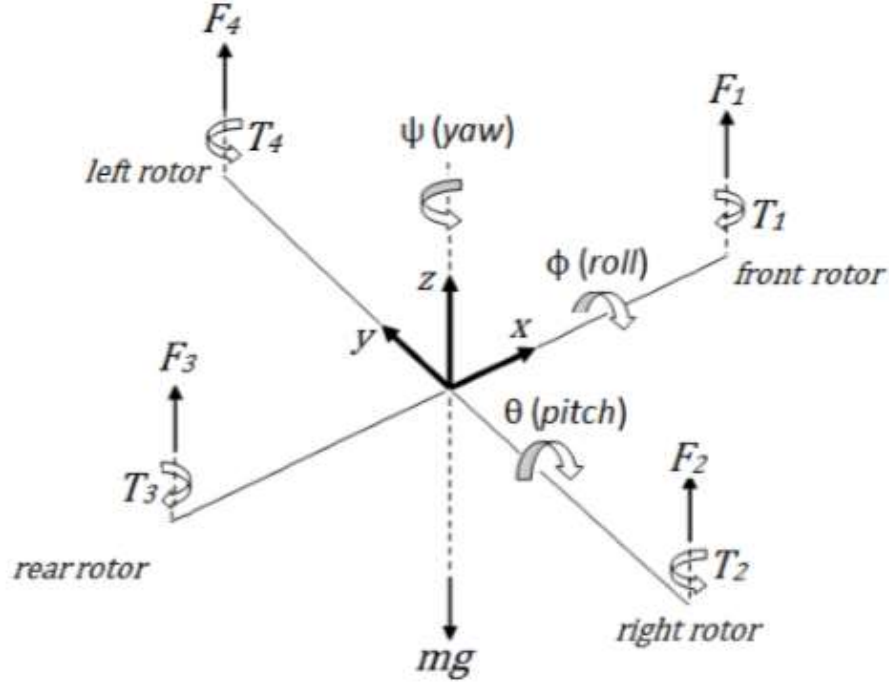


Figure 2.2 Force and Torque Generated by Each Propeller and Rotor Configuration

The physical model of the the quadrotor are shown as in Figure 2.2. Thrust forces generated by each rotor are show as F_1, F_2, F_3, F_4 and the moments generated by each rotor are shown as T_1, T_2, T_3, T_4 in Figure 2.2. The distances between rotors and the center of gravity of the quadrotor are equal and shown as b_d .

In Equations (2.1), (2.2), (2.3) and (2.4) represent four different combinations of forces and moments which are expressed in Figure 2.2,

$$U_1 = F_1 + F_2 + F_3 + F_4 \quad (2.1)$$

$$U_2 = b_d(F_4 - F_2) \quad (2.2)$$

$$U_3 = b_d(F_3 - F_1) \quad (2.3)$$

$$U_4 = T_2 - T_1 + T_4 - T_3 \quad (2.4)$$

As can be seen in Equation (2.1), U_1 is the total force generated by four propellers. It is directly related to the motion in the z-direction (altitude). U_1 is the force against gravity that causing the quadrotor to float in the air.

According to in Equation (2.2), U_2 is the differential moment between the right propeller and the left propeller. Therefore, it is link to the roll motion and angle ϕ represents roll motion. In Equation (2.3), U_3 is the differential moment between the front propeller and the rear propeller. Thus, it is related to the pitch motion and angle θ represents pitch motion. Besides, the motion in x and y directions are provided by changing angles ϕ and θ effect, respectively.

In Equation (2.4), U_4 is the net torque generated by four propellers. Hence, it is related to the yaw motion and angle ψ represents pitch motion. The front and rear propellers rotate in the clockwise direction, while right and left propellers rotate in the counterclockwise direction. All motion combination of quadrotor is illustrated in Figure 2.2. In addition, the heading of the quadrotor can be adjusted with changing of yaw angle ψ .

These U_1, U_2, U_3, U_4 parameters will be used in motor model control in Chapter 4.

2.3 Mathematical Model of Motor

It is necessary to define the relation among the propellers angular velocity and thrust and torque perform by propellers. F_i refers the thrust generated by i_{th} propeller. ω_i refers the angular velocity of i_{th} propeller [19],

$$F_i = k_n \omega_i^2 \quad (2.5)$$

In Equation (2.5), k_n is a constant which provides the relation angular velocity and thrust generated by propellers.

Let T_i shows the torque generated by i_{th} propeller. According to, torque generated by i_{th} propeller is defined as follows [19],

$$T_i = k_m F_i \quad (2.6)$$

In Equation (2.6), k_m relates thrust and torque generated by propellers and it is a constant. As k_m and k_n are constants, it may be concluded that the relation between thrust and torque generated by propellers and angular velocity of propellers is quadratic. Force F_i and torque T_i generated by each propeller are shown Figure 2.2. By using Equations (2.5) and (2.6), control inputs can be defined as U_1, U_2, U_3 and U_4 .

2.4 Aerodynamic Analysis of Propeller

The lift and drag forces are applied to the aerodynamic center of propeller because of the angular speed of the blade element of the propeller, that is illustrated in Figure 2.3. Lift forces are perpendicular to the relative wind, whereas drag forces are parallel to and in the same way as the relative wind. Each pair of propeller are rotating around different direction. However, in the hover position, each of them generates positive lift and neutral torque by the help of different pairs of the propeller.

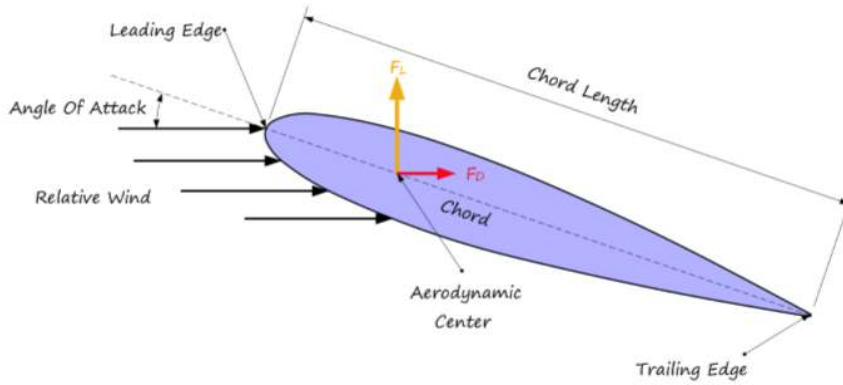


Figure 2.3 Forces on the Airfoil [20]

Those forces can be derived from the fluid dynamics by [20], and also using Blade Element Theory, detailed information about these forces is described in 2.4.1,

$$F_L = \frac{1}{2} \rho C_L A v^2 \quad (2.7)$$

$$F_D = \frac{1}{2} \rho C_D A v^2 \quad (2.8)$$

where ρ is fluid density, A is frontal area of the propeller, v is propeller linear velocity relative to fluid, C_L is dimensionless thrust coefficient and C_D is dimensionless drag coefficient.

In magnitude, the angular speed ω is equal to propeller velocity divided by the radius of propeller R . The lift force for a propeller can be rewritten as follows,

$$F_L = \frac{1}{2} \rho C_L A (\omega R)^2 \quad (2.9)$$

$$F_L = b \omega^2 \quad (2.10)$$

where b is thrust coefficient.

Drag force refers to a torque which is defined in magnitude as,

$$\tau_D = \frac{1}{2} \rho C_D A (\omega R)^2 \quad (2.11)$$

$$\tau_D = d \omega^2 \quad (2.12)$$

where d is drag coefficient.

Then, the complete motor torque due to the propeller drag and acceleration about the z-axis for a motor. It is given as follows,

$$\tau_M = \tau_D + I_R \dot{\omega} \quad (2.13)$$

The moment of inertia about the z-axis of the rotor represents I_R .

In the hover position, propellers trying to maintain the speed of the blades ($\dot{\omega} \approx 0$). Therefore, one of the complete torque component ($I_R \dot{\omega}$) can be ignored. Therefore, the simplified expression for the motor is,

$$\tau_M = d \omega^2 \quad (2.14)$$

2.4.1 Blade Element Theory

Blade Element Theory (BET) was first proposed by Drzwiecki in 1892 for the analysis of airplane propeller. BET assumes that each blade section acts as a two-dimensional airfoil to produce aerodynamic forces in Figure 2.4.

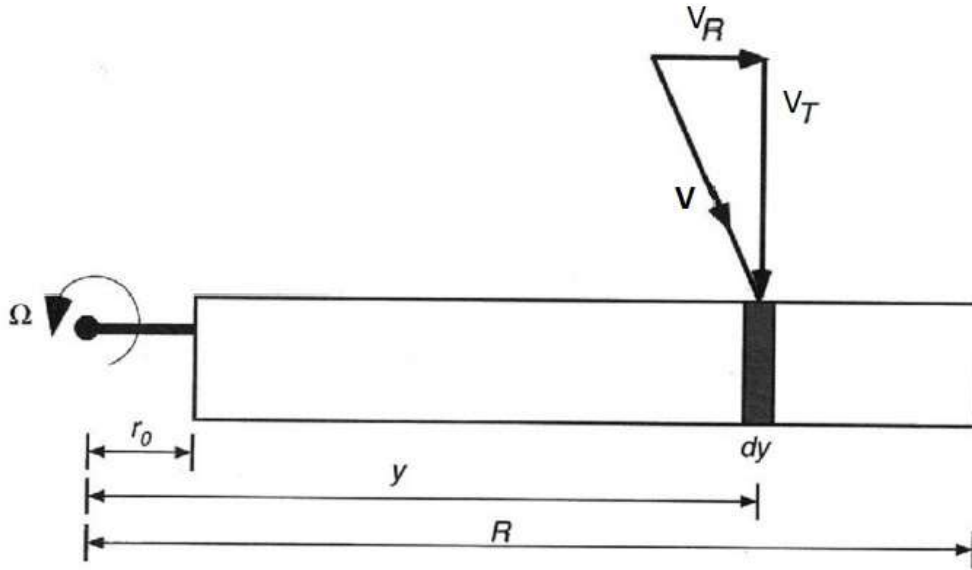


Figure 2.4 Drawing of airfoil [21]

The blade is then divided into non-interacting sections where all the computations are performed by using 2-D aerodynamics in Figure 2.5. Integration over the blade length gives the total thrust and total power [21].

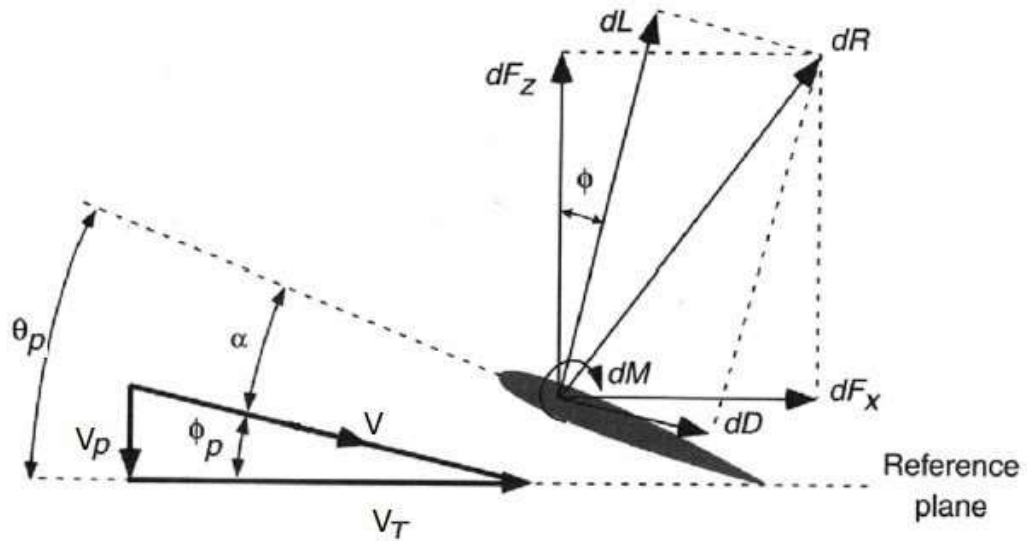


Figure 2.5 Airfoil cross section area and forces [21]

The airflow velocity V , has two vectors, which are V_T and V_p .

The in plane velocity shows in Equation 2.15. Ω is speed of blade and y is the distance of any point on the blade from the center of the rotor.

$$V_T = \Omega y \quad (2.15)$$

The out of plane velocity,

$$V_P = V_C + v_i \quad (2.16)$$

Therefore, the total velocity,

$$V = \sqrt{V_T^2 + V_P^2} \quad (2.17)$$

The relative inflow angle is,

$$\phi_p = \tan^{-1} \left(\frac{V_P}{V_T} \right) \quad (2.18)$$

If the blade element has a pitch angle of θ_p , the effective angle of attack α is,

$$\alpha = \theta_p - \phi_p = \theta_p - \tan^{-1} \left(\frac{V_P}{V_T} \right) \quad (2.19)$$

The incremental lift per unit span,

$$dL = \frac{1}{2} \rho V^2 c C_l dy \quad (2.20)$$

The incremental drag per unit span,

$$dD = \frac{1}{2} \rho V^2 c C_d dy \quad (2.21)$$

The lift force L and the drag force D can be resolved to get the forces perpendicular to and along to the rotor disk plane, respectively;

$$dF_z = dL \cos \phi_p - dD \sin \phi_p \quad (2.22)$$

$$dF_x = dL \sin \phi_p + dD \cos \phi_p \quad (2.23)$$

Accordingly, the elemental thrust, torque and power are,

$$dT = N_b dF_z \quad (2.24)$$

$$dQ = N_b dF_x y \quad (2.25)$$

$$dP = N_b dF_x \Omega y \quad (2.26)$$

N_b is the number of blades and we can relate all three with the lift coefficient C_l and the drag coefficient C_d ,

$$dT = N_b (dL \cos \phi_p - dD \sin \phi_p) \quad (2.27)$$

$$dQ = N_b(dL \sin \phi_p + dD \cos \phi_p) y \quad (2.28)$$

$$dP = N_b(dL \sin \phi_p + dD \cos \phi_p) \Omega y \quad (2.29)$$

If we assume that in plane velocity V_T is bigger out plane velocity V_P in hovering condition, $V_T \gg V_P$. Therefore, $\alpha, \theta_p, \phi_p \ll 1$. Hence,

$$V = \sqrt{V_T^2 + V_P^2} \approx V_T \quad (2.30)$$

$$\phi_p \approx 0 \Rightarrow \begin{cases} \phi_p = \tan^{-1}(V_P/U_T) \approx V_P/V_T \\ \sin \phi_p = \phi_p \\ \cos \phi_p = 1 \end{cases} \quad (2.31)$$

$$dD \ll dL, dD \sin \phi \approx dD \phi_p \approx 0 \quad (2.32)$$

The expression for Thrust, Torque and Power are shown in Equation 2.33, 2.34 and 2.35, respectively,

$$dT = N_b(dL \cos \phi_p - dD \sin \phi_p) = N_b(dL) \quad (2.33)$$

$$dQ = N_b(dL \sin \phi_p + dD \cos \phi_p) y = N_b(dL + dD)y \quad (2.34)$$

$$dP = N_b(dL \sin \phi_p + dD \cos \phi_p) \Omega y = N_b(dL + dD)\Omega y \quad (2.35)$$

Let's now nondimensionalize using for length R and for speed $V_{tip} = \Omega R$ r refers to radial coordinate of an arbitrary point on the blade, R is the rotor radius.

$$r = y/R \quad (2.36)$$

$$V_T/\Omega R = \Omega y/\Omega R = y/R = r \quad (2.37)$$

And the thrust, torque and power coefficients already defined,

$$dC_T = \frac{dT}{qA(\Omega R)^2} \quad (2.38)$$

$$dC_Q = \frac{dQ}{qA(\Omega R)^2 R} \quad (2.39)$$

$$dC_P = \frac{dP}{qA(\Omega R)^3} \quad (2.40)$$

The inflow ratio is shown in Equation 2.41,

$$\lambda = \frac{V_c + v_i}{\Omega R} = \frac{V_c + v_i}{\Omega y} \left(\frac{\Omega y}{\Omega R} \right) = \frac{V_p}{V_T} \left(\frac{y}{R} \right) = \phi_p r \quad (2.41)$$

Substituting the previous equations in the Thrust coefficient equation,

$$dC_T = \frac{N_b dL}{qA(\Omega R)^2} = \frac{N_b \left(\frac{1}{2} \rho V_T^2 c C_l dy \right)}{qA(\Omega R)^2} \quad (2.42)$$

$$dC_T = \frac{1}{2} \left(\frac{N_b c}{\pi R} \right) C_l \left(\frac{y}{R} \right)^2 d \left(\frac{y}{R} \right) \quad (2.43)$$

$$dC_T = \frac{1}{2} \sigma C_l r^2 dr \quad (2.44)$$

The same method is applying to obtain Power coefficient,

$$dC_P = dC_Q = \frac{dQ}{qA(\Omega R)^2 R} = \frac{N_b (\phi_p dL + dD) y}{qA(\Omega R)^2 R} \quad (2.45)$$

$$dC_P = dC_Q = \frac{1}{2} \sigma (\phi_p C_l + C_D) \left(\frac{y}{R} \right)^3 d \left(\frac{y}{R} \right) \quad (2.46)$$

$$dC_P = dC_Q = \frac{1}{2} \sigma (\phi_p C_l + C_D) r^3 dr \quad (2.47)$$

To find the total blade contribution for thrust and power, take the integral between the root and tip of the blade.

$$dC_T = \frac{1}{2} \int_0^1 \sigma C_l r^2 dr = \frac{1}{2} \sigma \int_0^1 C_l r^2 dr \quad (2.48)$$

If the blade is rectangular, c is constant.

For the torque and power coefficient,

$$dC_P = dC_Q = \frac{1}{2} \sigma \int_0^1 (\phi_p C_l + C_D) r^3 dr = \frac{1}{2} \sigma \int_0^1 (\lambda C_l r^2 + C_D r^3) dr \quad (2.49)$$

To evaluate the previous expressions, the following values should be obtained numerically. These values depend on the diameter and structure of the blade, the velocity, the Reynold number and the Mach number of the airflow.

- Inflow ratio $\lambda = \lambda(r)$
- Lift coefficient $C_l = C_l(\alpha, R_e, M)$
- Drag coefficient $C_d = C_d(\alpha, R_e, M)$
- Angle of attack $\alpha = \alpha(V_c, \phi_p, v_i)$
- Induced Velocity $v_i = v_i(r)$

These numerical values are given in detail in section 3.4 when selecting the propeller model.

3.1 Objective of Experiment

The purpose of this test bench system is to measure the lift force generated by a propeller. The total thrust in the quadrotor is modeled. Using the variable-pitch propeller and brushless DC motor, the lift force is measured both by changing motor rotational speed and propeller's pitch angle.

The method followed by during measurement;

1. The pitch-angle of the propeller is constant while the lift force is generated by changing the motor rotational speed.
2. The motor rotational speed is constant while the lift force is generated by changing the pitch-angle of the propeller.

The basic concept design of the thrust measurement test bench is shown in Figure 3.1.

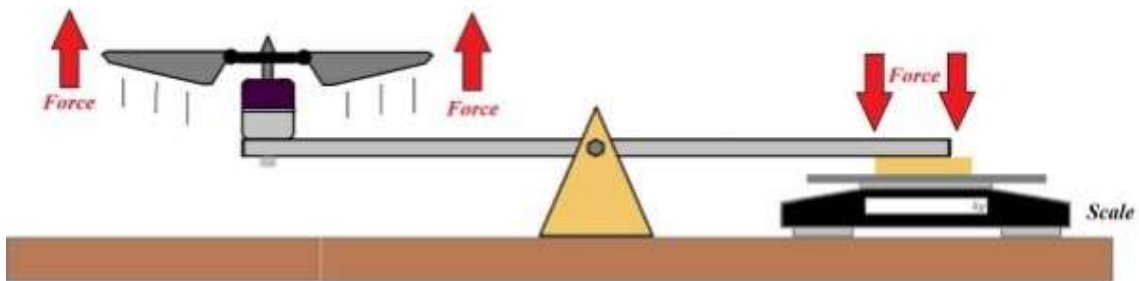


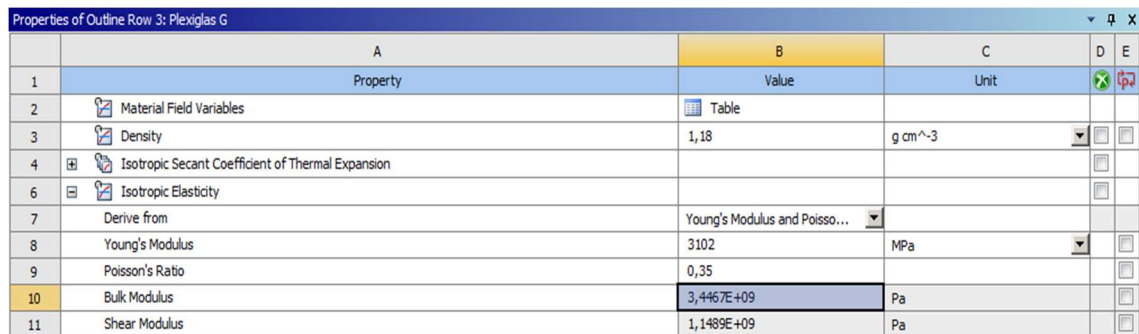
Figure 3.1 Concept Design of the Thrust Measurement Test Bench [23]

The thrust force is measured by the force sensor and verified with the precision scale. The brushless DC motor speed is measured by the Hall Effect sensor and 2 magnets. In addition, motor speed is verified by the optical digital sensor.

3.2 Test Bench Main Frame Strain Analysis

Before designing the test system, static structural analysis of mainframe is performed to ensure the endurance of the test bench. The aim of this section shows the effect of force on the stiffness of the structure. Mainframe material selection is made cautiously to avoid elasticity. Therefore, the material is chosen as Plexiglas G[®] and the minimum thickness of the frame is determined as 15 mm.

Plexiglas is a composite material and is analyzed as isotropic in force analysis. Thus, Shear modulus, Young Modulus and Poisson Ratio are the same value for each direction as in Figure 3.2 [24].



Properties of Outline Row 3: Plexiglas G			
	A	B	C
1	Property	Value	Unit
2	Material Field Variables	Table	
3	Density	1,18	g cm ⁻³
4	Isotropic Secant Coefficient of Thermal Expansion		
6	Isotropic Elasticity		
7	Derive from	Young's Modulus and Poisso...	
8	Young's Modulus	3102	MPa
9	Poisson's Ratio	0,35	
10	Bulk Modulus	3,4467E+09	Pa
11	Shear Modulus	1,1489E+09	Pa

Figure 3.2 Material Property of Plexiglas G[®]

In analysis, ANSYS Workbench software is used by applying Finite Element Method. While the model is being created, contact types are defined as linear, such as no-separation and bonded contacts are selected in the FEM analysis. Other contact types are Non-Linear contacts which are used in Non-Linear Analysis.

In addition, mesh building is crucial to solve mathematical model. Element Quality, Jacobian, Skewness and Orthogonal Quality are important to decide the best meshing. The significant feature is Jacobian value and it should be between 0 with 1 and near to 0 have good mesh-quality. The boundary conditions are defined as force and fixed support.

The force is defined 3 N and solved, as can be seen in Figure 3.3. A maximum force of 1 N was observed in the tests. The test bench was simulated with 3 N to ensure durability.

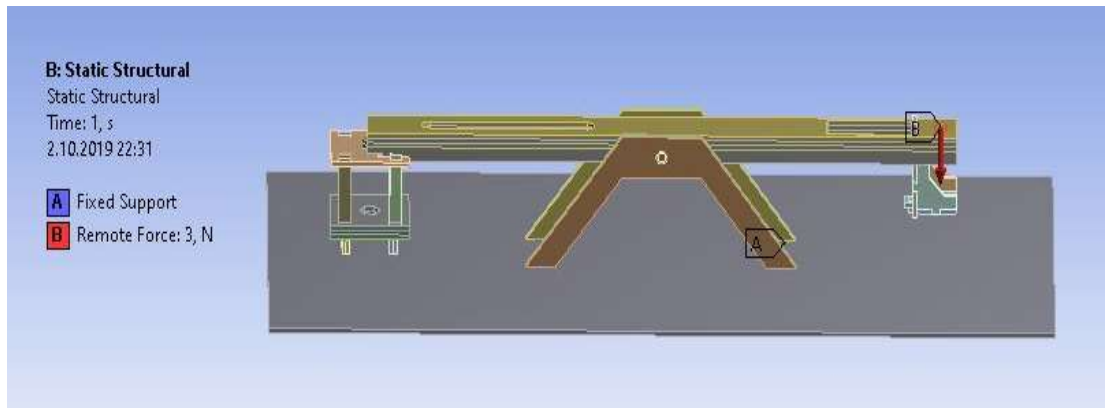


Figure 3.3 The Boundary Conditions of Test Bench System and the Force

Maximum strain values are obtained as 0.00051 mm/mm. This result of the analysis is shown in Figure 3.4.

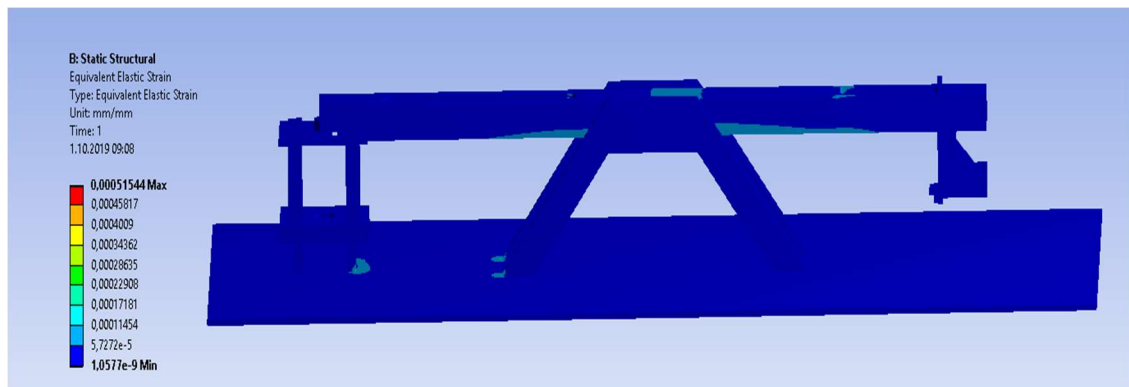


Figure 3.4 Strain Analysis Result

When the 3 N vertical force is simulated, a maximum strain value calculates 0.00051 mm/mm at the other end of the test device. This force is 3 times higher than the measured lifting forces. The value of the lateral forces is very small when compared to the lift force. So the lateral forces are neglected.

Ground effect is the change of flight characteristics of an aircraft when flying close to the ground or another surface. In test model, there is a space under the propeller area of the test apparatus, minimizing the ground effect as much as possible.

3.3 DC Motor

Brushless DC motors are generally used in UAVs and the reason for preference is their efficiency reaches up 99%. It provides 50% longer flight time compared to standard brush DC motors. The KV value indicates the revolution per voltage applied to the motor.

Brushless DC motors mainly come in two types: interior and exterior rotors. In interior types, permanent magnets are attached to inside surface of the rotor and vice versa for exterior rotors.

Generally, exterior rotors are used in many air vehicles due to the ease of cooling and assembly of blades, and reducing the cost of permanent magnet production which is attached to the stator.

In other vehicles that run on land and water, internal rotors are preferred in order to protect the interior from moist and dust.

Since torque is a factor of force between permanent magnets and coil in an electric motor, higher torque values can be achieved by the increase of each. By this logic, large diameters in motors lead to high torques compromising rotational speed. Therefore, it has been advised selecting lesser diameters for high KV values and greater diameters for less KV.

AEO A28M 2200KV brushless DC motor is used in this test bench. As can be seen in Figure 3.5, it weighs 0,063 kg including 7-inch propellers. It generates power up to 270 Watt. Motor drives can be operated nominal 27 Amps when supplied with 12V DC power.



Figure 3.5 Brushless DC motor

Technical specifications of brushless DC Motor are shown Table 3.1

Table 3.1 Technical Specifications of Brushless DC Motor

Brand	AEO
Rotation Speed (No Load)	7V 1,45A 14700rpm, 8V 1,57A 17400rpm, 1,84A 218000 rpm
Max. Current	27A
Max. Power	270W
Motor Dimension (Diameter x Length)	27,5 x 26,5 mm
Weight (Motor, Variable Pitch & Prop)	63 grams
ESC	20 - 30 A

3.4 Propeller Model

The propellers in the aircraft have two types of structure. There are one-piece propellers with fixed pitch angle commonly used in aircraft and quadrotor, and multi-piece propellers with variable pitch angle generally used in helicopters. Variable pitch angle propellers are used in the studies since the basis of the study is variable pitch angle control.

The 7-inch propellers are used in this study.

The material of the propellers is also quite important. Before the development of plastic production technologies, hand-made wooden propellers were used. Then plastic propellers start to be widely used. High-tech and cost-effective propellers such as with carbon-fiber are used in situations where high performance is required minimizing the inertia of the rotating propeller.

Plastic propellers are preferred in this study.

The pitch values of the propellers should be selected according to the desired level of the speed. High pitch value propellers are preferred in high-speed flights because of their low speed and high airlift force. However, the diameter of the propeller is as important as the pitch value. Large diameter propellers have higher efficiency than smaller diameter propellers that will apply the same force. For this reason, the use of large diameter propeller is preferred in low-speed flights. In contrast, small-diameter propellers are preferred in high-speed flights.

On February 7, 1922, Wallace Rupert Turnbull patented the variable pitch propellers. This patent is known as one of the essential patents in the aviation industry. This innovation allows the control of propeller pitch changes according to flight conditions or vehicle weight.

Variable pitch propeller is a system in which the blade angles can be individually adjusted. The shaft of the motor used in this system has a hole, and the rod which controls the pitch angles is passed through this shaft. By moving this rod forward or backward along the motor shaft, the pitch angle can be changed.

To control the pitching motion of propeller, the designed mechanism shown in Figure 3.6 and the variable-pitch mechanism in Figure 3.7 are used in the thesis. The control arm is connected to the propeller shaft through a linear actuator. The amount of the pitch is controlled by a linear actuator.

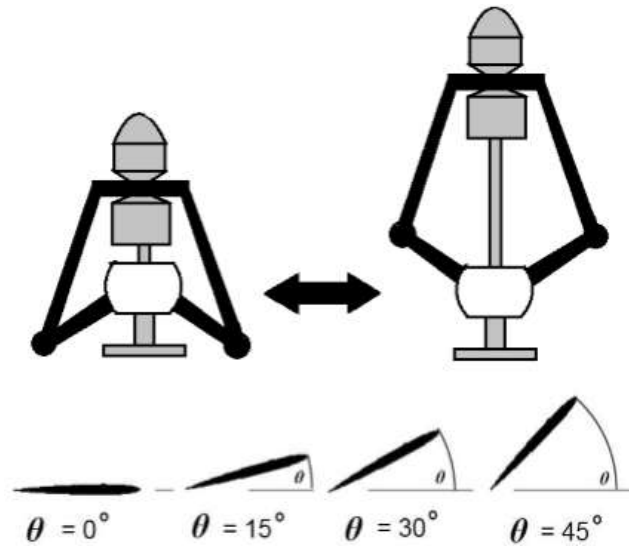


Figure 3.6 Propeller Pitch Motion [23]



Figure 3.7 Propeller Pitch

Technical specifications of variable pitch unit used in this test apparatus are shown in Table 3.2.

Table 3.2 Technical Specifications of Variable Pitch Unit

Model	4D Hollow Variable Pitch
Dimensions	140x70x19 mm
Weight	25 gr

The analytical analysis of variable-pitch actuation needs a detailed study of the aerodynamics of the propeller. Propellers operated on the variable-pitch rotor have 7-inch diameter tapered and symmetric blades as shown in Figure 3.8. The coefficients of all propeller structures are selected from NACA values, which has been analyzed and published-free by NASA and accepted worldwide. To determine the lifting and drag coefficients of the propellers to be used in the analysis, the Reynolds number and Mach number must be selected according the propeller features. NACA 0009 airfoil is chosen to model the propeller. Since the maximum thickness of chord ratio is 0,899. The Mach number is 0.25 when the blades rotate at 8000 RPM. Thus the Reynolds number is about 100000.



Figure 3. 8 The Variable-Pitch Mechanism and Corresponding Propellers

Table 3.3 shows aerodynamic coefficients for propeller blades according to NACA.

Table 3.3 Propeller Aerodynamic Coefficients According to NACA

C_{L0}	C_{La}	C_{Lmin}	C_{Lmax}	C_{D0}	C_{D2u}	C_{D2l}	$C_L C_{D0}$	RE_{ref}	RE_{exp}
0.0	2.87	0.0	0.7	0.01	0.0408	0.0408	0.0	100000	-0.5

3.5 Electronic Speed Controller

Electric speed controllers are used to control the brushless DC motor. It is used to transmit high currents against high motor forces to the motor in a controlled manner and to set the motor speed desired by the user. Electronic speed controllers also have values that show their main features. In general, the features used in the selection of electronic speed controllers are listed as follows;

Voltage: It is the maximum voltage value of the electronic speed controller. Electronic motor controller will be damaged if power supplier value is above this value.

Maximum Instantaneous Current: It is the maximum instant current value supported by the electronic speed controllers. If motors are connected to the electronic speed controllers, which can draw current above this value, they will be damaged. In this expression that the instant term varies, and it should be written in parentheses. This value should not be considered as a definite limit since it depends on many variables.

Maximum Continuous Current: Electronic speed controllers are able to provide this current for a long time. However, if this value is exceeded for a long time, the controller may be damaged. Since helicopters, rotary-wing UAVs and slow-flying aircraft operate under continuous load, and therefore an electronic speed controller should be selected considering the maximum continuous current value.

Maximum Speed: The speed motor specified here may not have a real speed of the motor; this is because the number of poles is indicated in addition to the speed. It has a maximum speed in inverse proportion to the number of poles.

Example: 240,000 rpm and a 2-pole controller can operate on a 4-pole motor with a maximum of 120,000 rpm. The reason for this is shown in the following chapters that explain the operating logic of the electronic speed controller.

PWM (Pulse Width Modulation): The frequency ranges of the input signal to the electronic speed controller. The electronic speed controller does not operate at lower or higher frequency signals than the specified frequency range. This value is linked to the signal from your radio device or drive controller card.

BEC (Battery Eliminator Circuit): It reduces the voltage from the power supply or battery and feeds the control receiver. The voltage of the batteries which are usually used for the motor is higher than the operating voltage of the control receiver. Therefore, to avoid damage to the receiver, this voltage value is lowered by BEC and delivered to the receiver.

In addition to the above basic features, the physical characteristics of the electronic speed controller are indicated. Especially weight is one of the most important features. In this thesis, Skywalker 40A ESC is selected and it is shown in Figure 3.9. The maximum current capacity is 40 amps and the input frequency is 1 kilohertz. The average weight of the ESC is 31.5 grams and its dimensions are 70x25x10 mm.



Figure 3.9 Electronic Speed Controller

3.6 Hall Effect Sensor

Hall Sensors are magnetically operated semiconductor sensors. In order to know the working principle of this sensor, it is necessary to Hall Effect.

When electrons flow from a semiconductor, a magnetic field perpendicular to the direction of current is applied, the electrons are concentrated in a specific region. This causes a voltage to form at the other ends of the semiconductor. This is called a hall effect. The value of the voltage generated at the semiconductor by the Hall effect depends on the magnetic field and the proximity of the object to the sensor. The continuous change of the magnetic field provides a square wave signal at the sensor output. The Hall Sensor can be installed in various ways. The sensor uses for counting speed, positioning, coding, etc. by sensing metal and magnetic materials.

The test bench is equipped with Keyes KY-003 hall effect sensor as shown in Figure 3.10. This sensor operating voltage is 5V and its material is PCB.

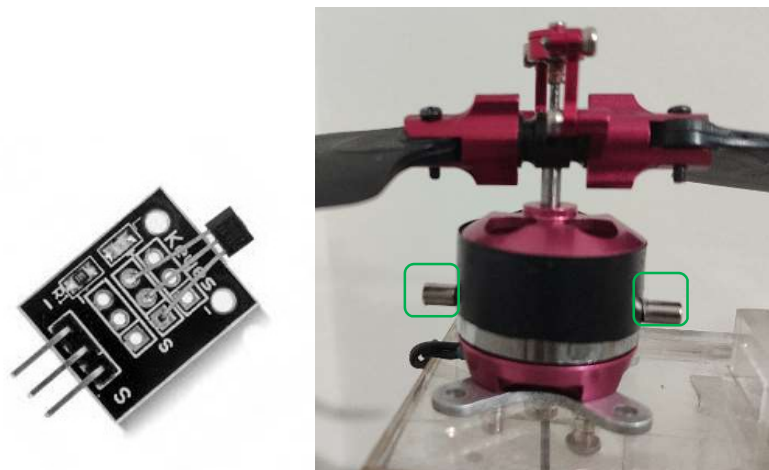


Figure 3.10 Hall Effect Sensor and Magnets

The hall effect sensor is used for the brushless DC motor speed measurement. This sensor requires magnets fixed to housing of the outer motor. The precision of measurement is directly proportional to the amount of magnets on the motor housing. Two magnets provide adequate measurements for the tests and they are also shown in Figure 3.10.

3.7 Force Sensor

Force sensors are composed of materials whose resistance varies according to the applied pressure. It is used to measure force. Although these materials are referred to as force-sensitive resistance, the material is actually pressure-sensitive. However, it is still possible to measure force.

Force sensitive resistor is adding test bench system to measure the lift force generated by propeller. It is shown in Figure 3.11.

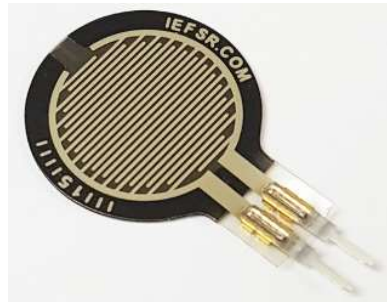


Figure 3.11 Force Sensitive Resistor Sensor

The resistance of FRS's changes as more pressure is applied. The sensor looks like an infinite resistor (open circuit) when there is no pressure and when the pressure rises, the resistance decreases. This graph, which is shown in Figure 3.12, demonstrates approximately the resistance of the sensor at different force measurements. It is essential to note that the graph is not really linear. Therefore, pre-test process the sensor should be calibrated with weight and multimeter.

The ambient temperature during the experiment is 25°C and constant.

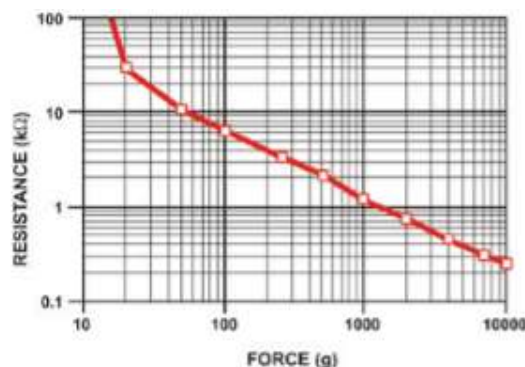


Figure 3.12 The Resistance/The Force Graph of FSR [25]

3.8 Test Bench Model

Lift force measurement is done with below test bench in Figure 3.13. The propeller pitch angle is changed and the impact of this change on the lift force is observed. The hall effect sensor measures the brushless DC motor speed. The force sensor measures the lift force on the propeller. The brushless DC motor is controlled by Arduino using ESC. DC motor speed is set by a potentiometer. The pitch angle of the propeller can be set at any value by moving actuator shaft vertically. 1° change in pitch angle can be obtained by moving shaft by 0.5 mm. For the purpose of this study, the pitch angle is kept within the range of 0-20°.

The schematic representation and connection of the test apparatus is shown in Figure 3.14.

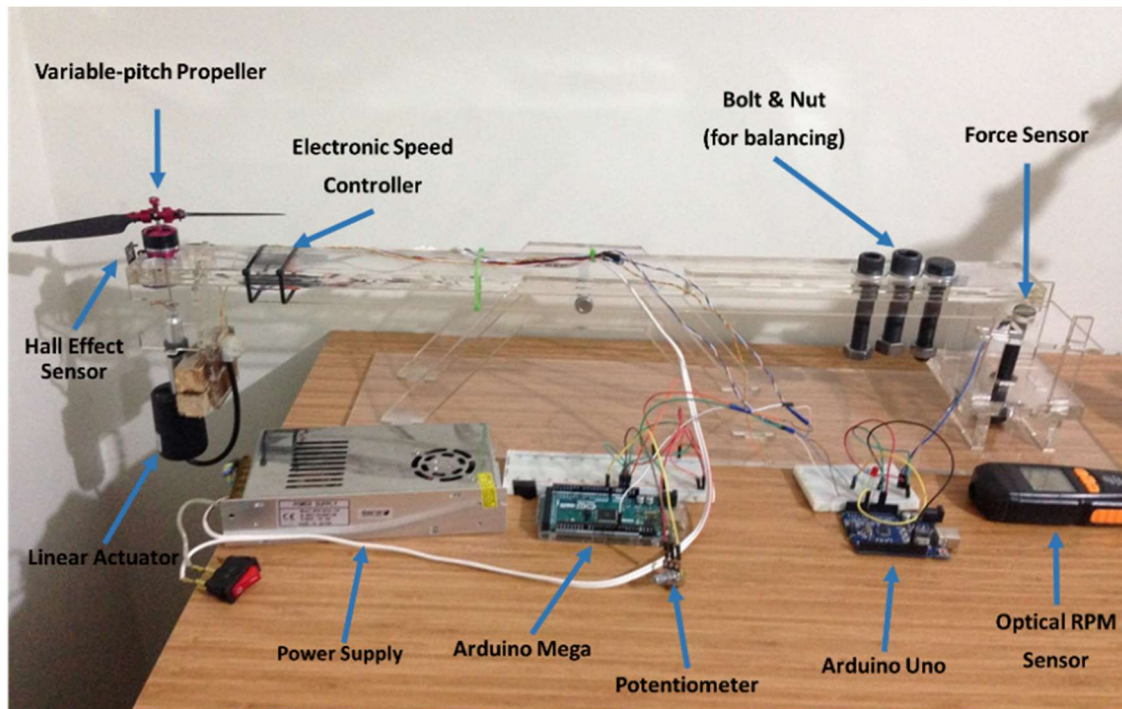


Figure 3.13 Test Bench

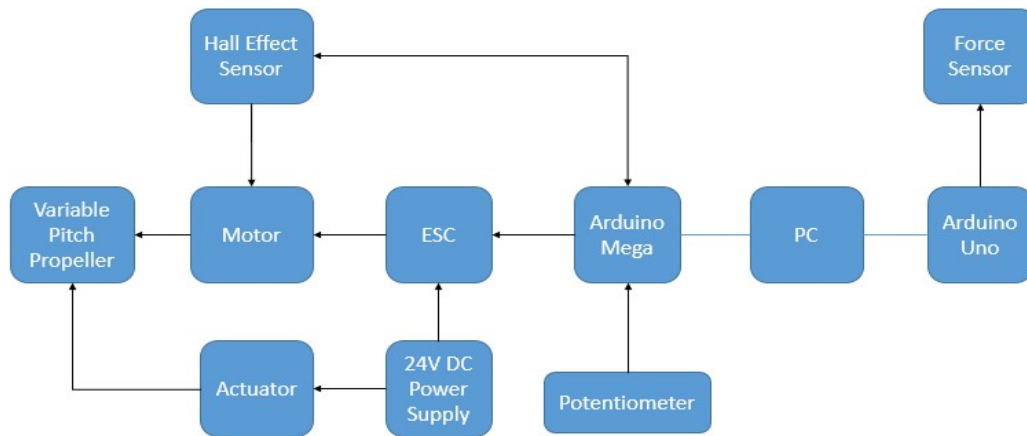


Figure 3.14 Schematic Representation of Test Apparatus

Types of equipment of test bench are listed in Table 3.4.

Table 3.4 Types of Equipment of Test Bench

No	Component	Type
1	Main Frame	Custom
2	Variable Propeller Pitch	4D Metal Variable Pitch
3	Hall Effect Sensor	Keyes 003
4	Electronic Speed Controller	Skywalker 40A
5	Force Sensor	Interlink 402 model
6	Arduino Mega 2560 R3	Arduino
7	Arduino Uno	Arduino
8	Brushless DC Motor	AEO C20 1550KV EVP
9	7-inch Propellers	OM438
10	Linear Actuator	SKA-03-30-D2
11	Potentiometer	10 K Spike

12	Power Supply	NTS-0515-12V Keskinler
13	Thermometer	H106B - TT Technic

All sensors, motor, and ESC are compatible with Arduino.

It is also possible to measure torque values in the test setup, but since torque values will not be used in this thesis, only the lift force measurement is performed.

3.9 Findings of Lift Force Measure

The obtained lift forces by adjusting the pitch angle of the airfoil and the motor rotation speed are presented in Table 3.5 and plotted in Figure 3.15.

Table 3.5 Lifting Forces Caused by Angle and Speed Changes

Rotational Speed (rpm)	Propeller Pitch Angle (°)				
	0°	5°	10°	15°	20°
1500	4,02x10 ⁻³ N	15,30x10 ⁻³ N	26,49x10 ⁻³ N	61,80x10 ⁻³ N	62,98x10 ⁻³ N
2000	6,28x10 ⁻³ N	22,07x10 ⁻³ N	41,20x10 ⁻³ N	88,88x10 ⁻³ N	89,76x10 ⁻³ N
3000	16,78x10 ⁻³ N	53,56x10 ⁻³ N	92,41x10 ⁻³ N	214,84x10 ⁻³ N	215,72x10 ⁻³ N
4000	27,76x10 ⁻³ N	88,58 x 10 ⁻³ N	154,21x10 ⁻³ N	354,63x10 ⁻³ N	355,51x10 ⁻³ N
5000	40,32x10 ⁻³ N	125,96x10 ⁻³ N	214,84x10 ⁻³ N	504,72x10 ⁻³ N	505,61x10 ⁻³ N
6000	48,27x10 ⁻³ N	153,04x10 ⁻³ N	261,04x10 ⁻³ N	615,09x10 ⁻³ N	615,68x10 ⁻³ N
7000	61,31x10 ⁻³ N	188,65x10 ⁻³ N	311,96x10 ⁻³ N	718,09x10 ⁻³ N	718,68x10 ⁻³ N
8000	75,73x10 ⁻³ N	233,09x10 ⁻³ N	396,42x10 ⁻³ N	934,11x10 ⁻³ N	934,40x10 ⁻³ N

The lift forces observed at 0° are equal to those of fixed pitch propellers.

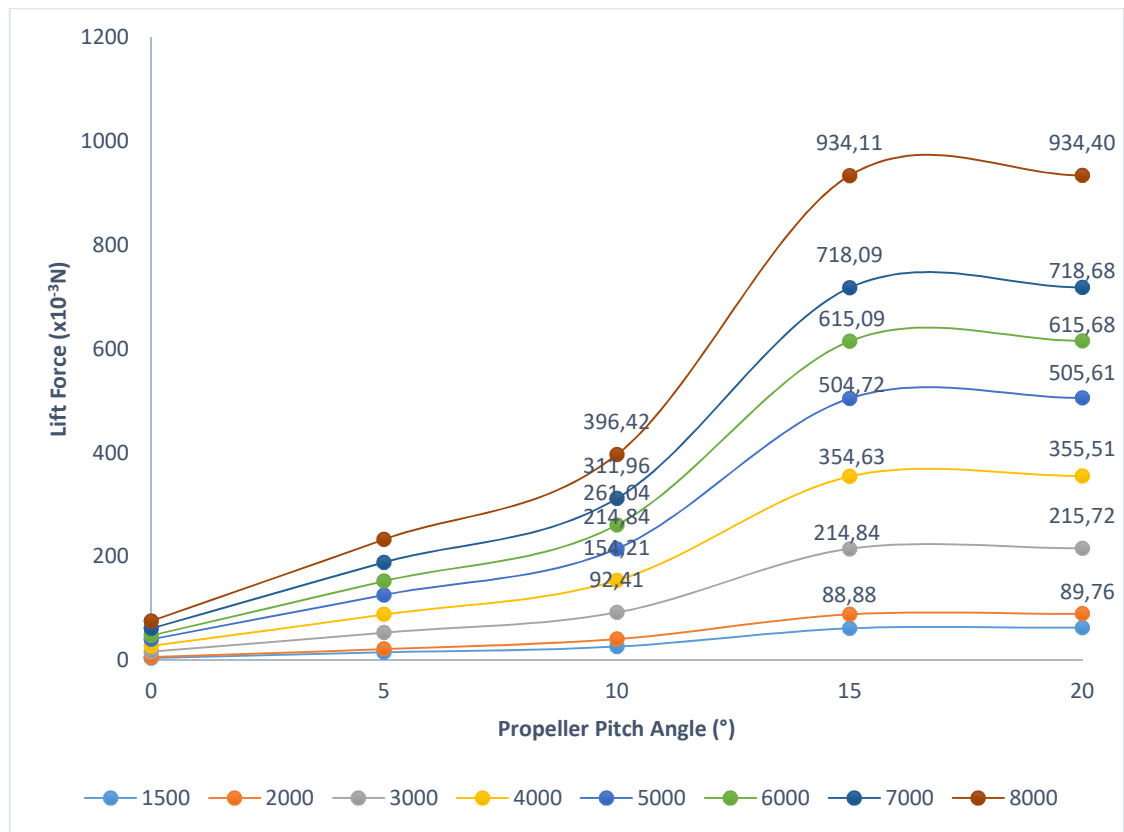


Figure 3.15 Lift Force – Pitch Angle – Rotational Speed (rpm) Graph

Figure 3.15 shows an extrapolation of a 7-inch-propeller at 0-20 degrees pitch angle and 0-8000 motor rotational speed. The change in the range of 0 and 10 degrees in pitch angle causes an almost linear increase in lift force, but not much. Between 10 and 15 degrees the force increases exponentially. However, there is almost no change between 15-20 degrees and higher. This is due to a phenomenon called stall which occurs when airflow over the blades is unsteady and turbulence is present causing significant drop in lift force generated. Therefore, optimal working pitch angle of variable pitch propellers is between 10-15 degrees as can be inferred from Figure 3.15.

The maximum lift force is about 1 N obtained at 8000 rpm and 15 degrees. In another example, the propeller has provided a sufficient lift force at 5000 rpm and pitch angle of 15 degrees enough to hover a quadrotor weighing 205 grams.

The gains in every unit change in pitch angle is so significant that 1 degree change in pitch angle between 10-15 degrees generates equal or greater lift force than a fix

pitched propeller at same rpm with the ease of 0.5 mm linear move in propeller shaft.

Trends in change of lift force by change in pitch angle shows similarities with the results obtained in [16].

In addition, while pitch angle is constant and equal 0° , the lift force on the propeller is directly related to the motor rotational speed as shown in Figure 3.16.

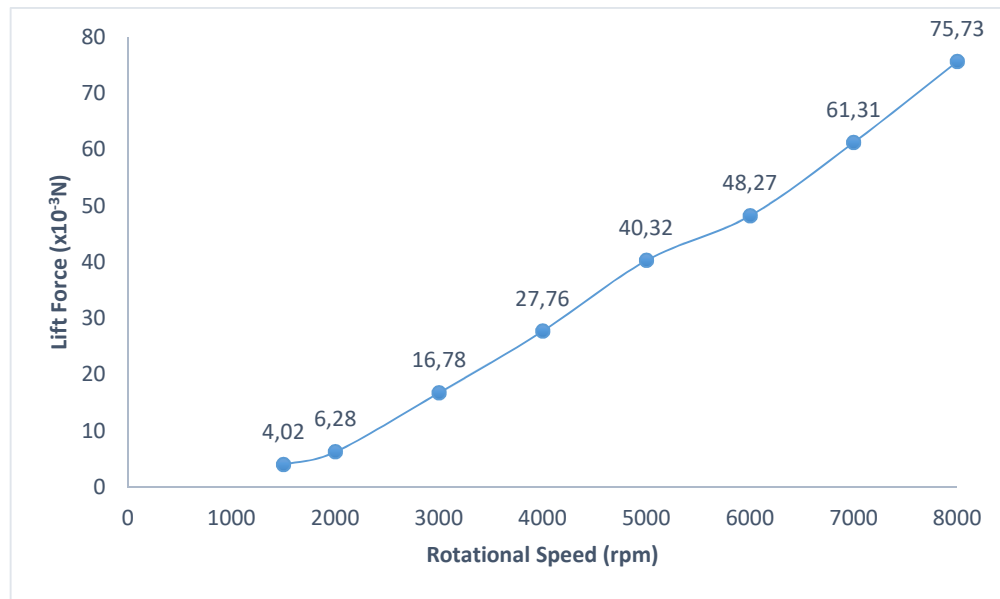


Figure 3.16 Lift Force – Rotational Speed (rpm) Graph (Pitch Angle is constant and equal 0°)

Fixed pitch propellers generate lift forces in proportion to its rotational speed as shown in Figure 3.16. Such linear gains is too modest compared to exponential gains in variable pitch propellers. In this respect, when lift or agility is a concern it is the variable pitch propeller that would bring optimal solutions.

In an effort to understand what is compromised in exchange of obtaining greater lift force looking at energy consumption at each pitch angle is essential. One of such study is compiled in [27]. It explains the endurance performance of a variable pitch propeller at the same battery capacity. According to this, for the given battery capacity of 5000 mAh the pitch angle is changed from 3-15 degrees. Juxtaposing these values with the values measured in Figure 3.15, at 8000 rpm an increase in lift force from $396,42 \times 10^{-3}$ to $934,11 \times 10^{-3}$ N (%136) by changing pitch angle from 10 to 15 degrees reduces the endurance time by just 12,61%.

4.1 Motor Model Control

In this thesis, motor is defined as a first-order differential equation in [26],

$$\frac{d\omega_i}{dt} = k_g(\omega_{i,des} - \omega_i) \quad (4.1)$$

The relation expressed in Equation (4.1) is used as a motor model in simulations. k_g is defined as motor gain and it refers to the time delay of the motor. The numerical value of k_g is found as 20 s^{-1} in [26]. $\omega_{i,des}$ refers to the desired angular velocity of the propellers, and $\omega_{i,des}$ determined by the control system. ω_i refers to the actual angular velocity of the propellers generated by motors.

By this equation creates a delay between the desired angular velocity and the actual angular velocity when modeling of the motor. Thus, the modeled motor system becomes more realistic.

$$F_i = k_n \omega_i^2 \quad (4.2)$$

$$T_i = k_m F_i \quad (4.3)$$

The relation between the angular velocity of the propellers and the control inputs U_1, U_2, U_3, U_4 is obtained to require to complete the motor model. In Equation (4.2), (4.3) in F_i and T_i are defined previously in Equations (2.1), (2.2), (2.3) and (2.4) in Section 2. The relation between the forces and moments in these equations and the angular velocities of propeller are determined by Equation (4.2) and (4.3). k_n represents to thrust factor and k_m represents to torque factor. Besides k_n and k_m are constants. These constants are related to cross section profile, length, width and angle of the attack of airfoil. Airfoil constants are obtained in NACA [22].

4.2 Stability of Motor Model

The stability of the system is determined to ensure the accuracy of the design model. Thus, the transfer function of the model must be found and its roots examined. The roots of the system are found by the root locus method.

The dynamic model of motor represents as a first-order differential equation,

$$\dot{\omega}_i = k_g(\omega_{i,des} - \omega_i) \quad (4.4)$$

Time variant function is defined,

$$\frac{d\omega_i(t)}{dt} = k_g(\omega_{i,des}(t) - \omega_i(t)) \quad (4.5)$$

Laplace function implements Equation 4.5 and shows as following,

$$\mathcal{L}\left\{\frac{d\omega_i(t)}{dt}\right\} = \mathcal{L}\{k_g(\omega_{i,des}(t) - \omega_i(t))\} \quad (4.6)$$

$$s\omega_i(s) - \omega_i(0) = k_g s\omega_{i,des}(s) - k_g s\omega_i(s) \quad (4.7)$$

Transfer Function is the ratio of the output of a system to the input of a system,

$$\text{TF: } \frac{\omega_i}{\omega_{i,des}} = \frac{k_g}{(s+k_g)} \quad (4.8)$$

The roots of the obtained Transfer function are shown in Figure 4.1.

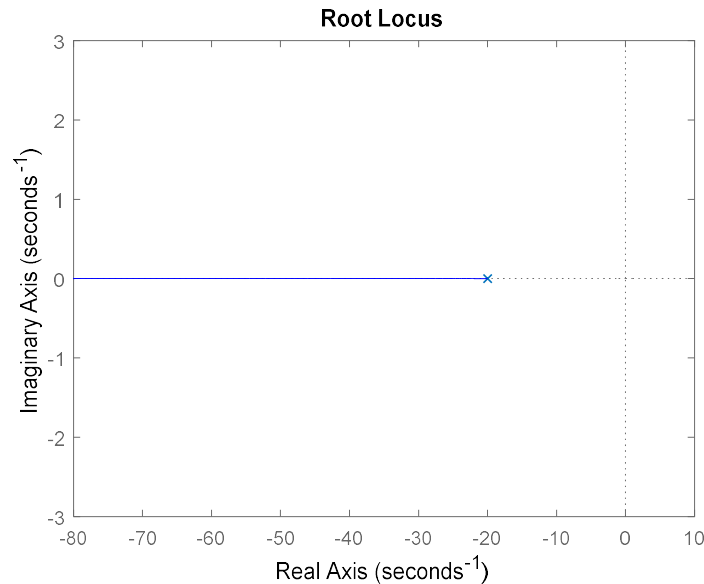


Figure 4.1 Motor Model Root Locus

When the roots of the system are examined, the system is stable against any force to be applied. Therefore, PID control of system can be designed.

In addition, step function is given to the system and the step response of the motor model is shown in the Figure 4.2.

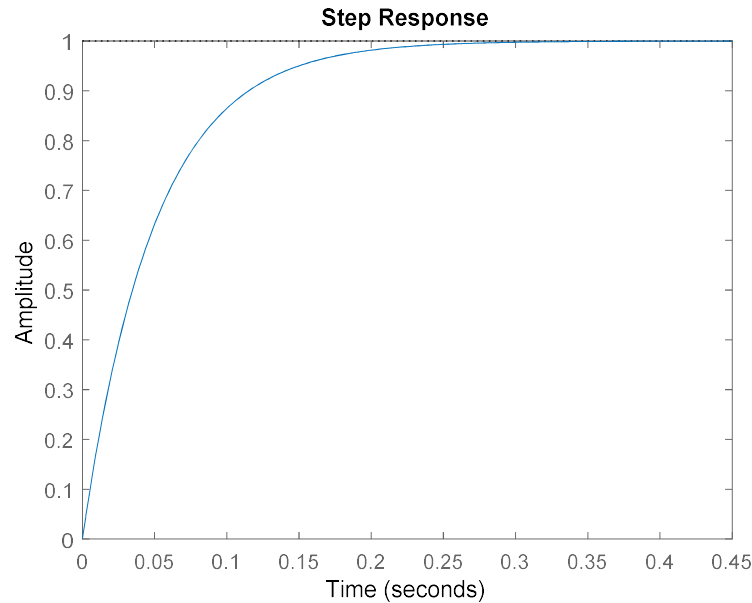


Figure 4.2 Step Response of Motor Model

As can be seen in Figure 4.1 and Figure 4.2, the stability of the motor model is assured.

4.3 PID Model

Proportional-integral-derivative (PID) controller, control loop method is a commonly used feedback controller method in industrial control systems. PID controller continuously calculates an error value, that is, the difference between the desired system state and the current system state. The controller attempts to minimize the error by adjusting the process control input. The classical PID controller structure is shown in Figure 4.3.

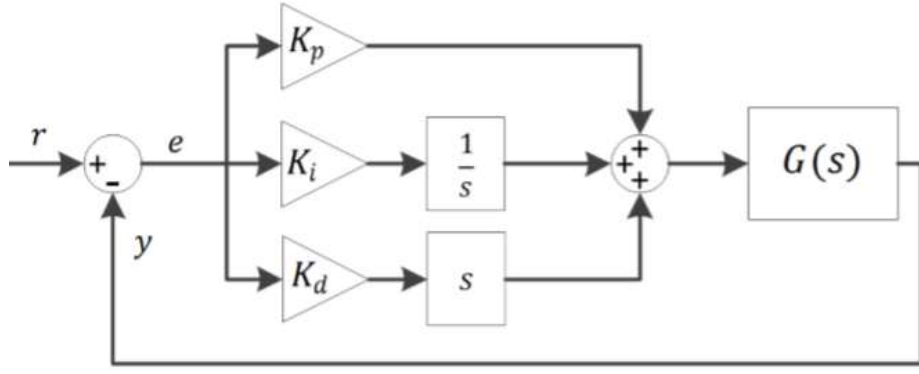


Figure 4.3 Typical PID Structure

When the PID control algorithm is examined mathematically, the output of the PID controller, t time, can be expressed as follows.

$$u(t) = P_u + I_u + D_u \quad (4.9)$$

In equation 4.9, P_u , I_u , D_u statements represent the effects of each PID term on output.

K_p represents proportional gain, e is error and t is time, the proportional term can be expressed as follows:

$$P_u = K_p e(t) \quad (4.10)$$

K_i represents integral coefficient, e is error, τ is integration variable and t is time, the integral term can be expressed as follows.

$$I_u = K_i \int e(\tau) d\tau \quad (4.11)$$

K_d represents derivative coefficient, e is error and t is time, the derivative term can be expressed as follows:

$$D_u = K_d \frac{d}{dt} e(t) \quad (4.12)$$

As a result, the output of the PID controller is calculated by taking the sum of the proportional term, integral term, and derivative term.

$$u = K_p e(t) + K_i \int e(\tau) d\tau + K_d \frac{d}{dt} e(t) \quad (4.13)$$

Fixed-pitch propeller and variable-pitch propeller system have been simulated in MATLAB-Simulink, general overview of both model is shown in Figure 4.4.

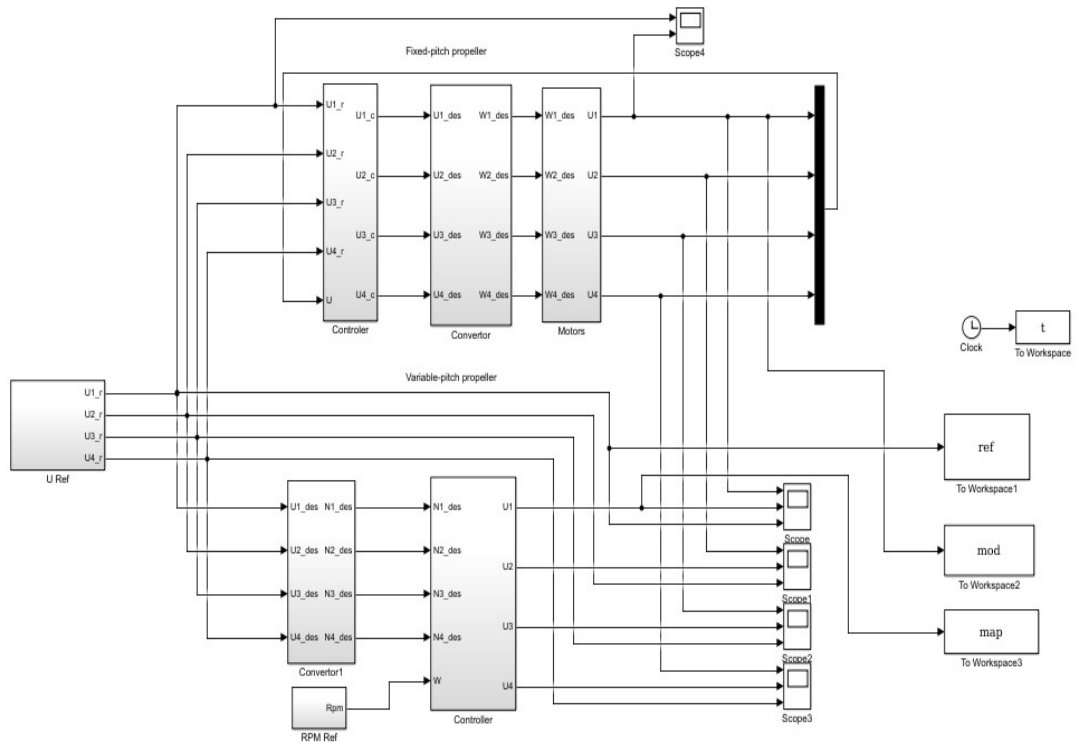


Figure 4.4 General Overview of Model

All the coefficients of the PID controller are taken as 0.005 as the initial value. Then, the Ziegler-Nichols method is used to find the appropriate control coefficients. The related coefficients and relations that should be used for Ziegler-Nichols method are presented in Table 4.1.

Table 4.1 Ziegler-Nichols Method

Control Type	K_p	K_i	K_d
P	$P_u/2$	-	-
PI	$P_u/2.2$	$T_u/1,2$	-
PID	$P_u/1,7$	$T_u/2$	$T_u/8$

The control coefficients proposed by Ziegler-Nichols method were obtained at the according to the Table 4.1. In this control method, starting with a P control coefficient, critical P value is searched, and thus critical period is obtained. The PID

control coefficients proposed by Ziegler-Nichols method is calculated and implemented on the system. The selection of coefficients is shown in Table 4.2

Table 4.2 Altitude Control with Ziegler-Nichols Method

Control Type	K_p	K_i	K_d
PI	15,45	0,83	-
PID	20	1	0,25

The fixed-pitch propeller and the variable-pitch propeller system is examined in Simulink, and the same PID gains implement both system to realize differences of altitude trajectory, it is shown in Figure 4.4.

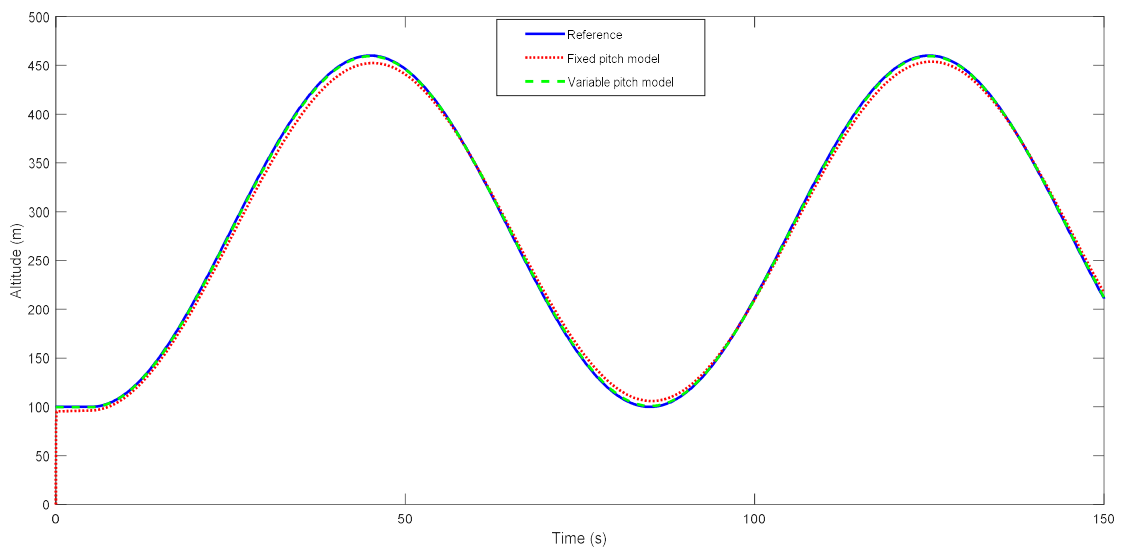


Figure 4.5 Altitude Trajectory

When fixed and variable pitch quadrotor models are compared based on their performance at altitude trajectory, variable pitch types outperform their counterparts as seen in Figure 4.5. Variable pitch propellers can follow the reference line perfectly because they generate the lift force by moving the actuator's shaft in a fraction of second that is negligible. In contrast, fixed pitch propellers respond much slower to the change in lift force required as they must achieve it by increasing motor rotational speed which takes longer time than that of variable pitch types.

5.1 Conclusion

The lift force is generated by changing the pitch-angle and motor rotational speed separately. Lifting force measurement is performed with this test bench and the results from tests are analyzed and compared.

The variable-pitch propeller and the fixed-pitch propeller quadrotor systems are modeled with the value in the test system by MATLAB–Simulink. Using the variable-pitch propeller for thrust variation rather than RPM regulation facilitates. Therefore, increasing the rate of change of the lift force generation. The blade element theory is used to estimate propeller thrust necessary to formulate rotor equation.

The use of unmanned aerial vehicles increases every day and they are already spread across many sectors. When there is so much interest, even a small efficiency improvement can lead to significant changes in how people live and interact with environment. Soon, the lighter and smaller types will emerge that come with lesser complexity and higher optimization to their application purposes. Scratching the surface of a topic of this much breadth, this thesis tries to unveil the potential of the use of variable pitch propellers that have many advantages over the fixed pitch propellers that were initially preferred for its mechanical simplicity and mostly targeting the hobbyists.

The results prove faster and accurate flights with high load carrying capacity can only be achieved by the use of variable pitch propellers as fixed pitched propellers today cannot satisfy the needs of tomorrow.

5.2 Future Work

Quadcopters are new concept and have many years ahead of it for development.

Variable-pitch propeller is used in the test measurement and the quadroter system is mathematically modeled. In the future studies, the quadroter prototype can be created by using four variable-pitch propeller. In order to fully comprehend and utilize the capabilities of the variable-pitch quadroter, future work should continue especially in the field of control design and trajectory generation. The variable-pitch quadroter should be able to perform a lot of incredible aerobatics and aggressive flight given the right control commands.

References

- [1] Goldman Sachs Research [Online]. Available:
<https://www.goldmansachs.com/insights/technology-driving-innovation/drones/>
- [2] M. J. Logan, J. Chu, M. A. Motter, D.L. Carter, M. Ol, and C. Zeune, "Small UAV research and evolution in long endurance electric powered vehicles.", in AIAA InfoTech @ Aerospace 2007 conference and Exhibit, vol. 2730, pp. 7–10, 2007.
- [3] K. Kawasaki, M. Zhao, K. Okada, and M. Inaba "MUWA: Multi-field universal wheel for air-land vehicle with quad variable-pitch propellers", in IEEE/RSJ International Conference on intelligent robots and systems (IROS), pp. 1880–1885, 2013.
- [4] J. Borenstein, "The HoverBot–An electrically powered flying robot." Unpublished white paper, University of Michigan, Ann Arbor, MI. Available FTP: <ftp://ftp.eecs.umich.edu/people/johannb/paper99.pdf>, 1992.
- [5] R. Cohen, D. Miculescu, K. Reilley, M. Pakmehr and E. Feron, "Online Performance Optimization of a DC Motor Driving a Variable Pitch Propeller." arXiv preprint arXiv:1310.0133 (2013).
- [6] E. Selim, Erol U. and M. Alci, "Dynamic Analysis and Control of a Quadrocopter." Applied Mechanics and Materials. Vol. 421. Trans Tech Publications, 2013.
- [7] Pang T. "Design, prototyping and autonomous control of gasoline-engine variable-pitch quadcopter.", National University of Singapore, 2016.
- [8] P. Pounds, R. Mahony, P. Hynes and J. Roberts, "Design of a four-rotor aerial robot." Proceedings of the 2002 Australasian Conference on Robotics and Automation (ACRA 2002). Australian Robotics & Automation Association, 2002.
- [9] E.A. Baran, C. Hançer, E. Çalıkoğlu, E. Duman, E. Çetinsoy, M. Ünel and M.F. Akşit, "İnsansız hava araçları için test düzeneği tasarımı ve üretimi." TOK'08 otomatik kontrol ulusal toplantısı, İstanbul, 2018.
- [10] Pongpaibul, B., "Experimental Flying Autonomous Vehicle.", MEng Cybernetics, 2001.
- [11] M. Orsag and S. Bogdan, "Hybrid control of quadrotor." 17th Mediterranean Conference on Control and Automation. IEEE, 2009.
- [12] P. Pounds and R. Mahony. ""Design principles of large quadrotors for practical applications." 2009 IEEE International Conference on Robotics and Automation, pp. 3265–3270, 2009.
- [13] G. d'Ambrosio and R. Navoni, Hg3 willy [Online-video]. Available:
<https://www.youtube.com/watch?v=M4uXmekZk-4>. July 2011.

- [14] H. Chen, variable-pitch quadrotor [Online-video]. Available: (<https://www.youtube.com/watch?v=fkSx3fSz0tE>), July 2011.
- [15] F. Emil and N. George, "Experimental model derivation and control of a variable pitch propeller equipped quadrotor", IEEE multi-conference on systems and control, Antibes, France, October pp. 8-10, 2014.
- [16] M. Cutler, N.K. Ure, B. Michini, and J.P. How, "Comparison of fixed and variable pitch actuators for agile quadrotors", AIAA Guidance, Navigation, and Control Conference (GNC), Portland, 2011.
- [17] E. Suicmez, "Trajectory tracking of a quadrotor unmanned aerial vehicle (uav) via attitude and position control", 2014.
- [18] D.P. Lopez, "Altitude Control in Microkopter Quadrotor", 2013.
- [19] M. Achtelik, "Nonlinear and adaptive control of a quadcopter", Dipl.-Ing. Dissertation, Lehrstuhl für Flugsystemdynamik, Technische Universität München, Garching, Germany, 2010.
- [20] A. Bramwell, G. Done, and D. Balmford, *Bramwell's helicopter dynamics*, American institute of aeronautics and astronautics, 2001.
- [21] F. Szolnoky Cunha, *Helicopter*, Instituto Superior Técnico, 2016.
- [22] M. Şanlıtürk, "Designing, implementation of test bench with PID control for variable-pitch propeller system.", 4th international congress on engineering, architecture and design, pp. 216-224, 2019.
- [23] A. Khalid, "Design, Development and Testing of Variable Pitch Propeller Thrust Measurement Apparatus-Freshmen Research Project.", Southern Polytechnic State University, 2012.
- [24] Plexiglass general information and physical properties, Altuglass international, [Online]. Available: <https://www.plexiglas.com/export/sites/plexiglas/.content/medias/downloads/sheet-docs/plexiglas-general-information-and-physical-properties.pdf>
- [25] Interlink 402 FSR datasheet, [Online]. Available: <https://www.trossenrobotics.com/productdocs/2010-10-26-DataSheet-FSR402-Layout2.pdf>
- [26] D. Mellinger, "Trajectory generation and control for quadrotors.", Ph.D. Thesis, University of Pennsylvania, Philadelphia, USA, 2012.
- [27] S. Sheng and C. Sun, "Control and optimization of a variable-pitch quadrotor with minimum power consumption.", College of automation engineering, Nanjing University of Aeronautics and Astronautics, Philadelphia, China, 2016.

Publications from the thesis

Contact Information: sanliturkmeahmet@gmail.com

Conference Papers

1. M. Şanlıtürk, "Designing, implementation of test bench with PID control for variable-pitch propeller system.", 4th international congress on engineering, architecture and design, pp. 216-224, 2019.

APPENDIX

Brushless DC Motor and Hall Effect Sensor Arduino Code

```
#include <Servo.h> //Using servo library to control ESC

Servo esc;

// read RPM and calculate average every then readings.

const int numreadings = 10;

int readings[numreadings];

unsigned long average = 0;

int index = 0;

unsigned long total;

volatile int rpmcount = 0;

unsigned long rpm = 0;

unsigned long lastmillis = 0;

void setup(){

  Serial.begin(9600);

  esc.attach(8); //Specify the esc signal pin

  esc.writeMicroseconds(1000); //initialize the signal to 1000

  attachInterrupt(0, rpm_bldc, FALLING);

}

void loop(){

  int val; //Creating a variable val

  val= analogRead(A0); //Read input from analog pin a0 and store in val

  val= map(val, 0, 1023,950,3600); //mapping val to minimum and maximum

  esc.writeMicroseconds(val); //using val as the signal to esc
```

```

if (millis() - lastmillis >= 1000){ /*Uptade every one second, this will be equal to
reading frecueny (Hz).*/

detachInterrupt(0); //Disable interrupt when calculating

total = 0;

readings[index] = rpmcount * 60; /* Convert frecueny to RPM, note: this works for
one interruption per full rotation. For two interrups per full rotation use rpmcount *
30.*/

for (int x=0; x<=9; x++){

    total = total + readings[x];

}

average = total / numreadings;

rpm = average;

rpmcount = 0; // Restart the RPM counter

index++;

if(index >= numreadings){

    index=0;

}

if (millis() > 11000){ // wait for RPMs average to get stable

    Serial.print(" RPM = ");

    Serial.println(rpm);

}

lastmillis = millis(); // Update lasmillis

    attachInterrupt(0, rpm_bldc, FALLING); //enable interrupt

}

}

```

```

void rpm_bldec(){ /* this code will be executed every time the interrupt 0 (pin2) gets
low.*/

    rpmcount++;

}

```

Force Sensitive Resister Sensor Arduino Code

```

pinMode(8, OUTPUT); //define where the pins are connected

int value;

void setup() {

    Serial.begin(9600);

    Serial.println('a');

    char a = 'b';

    while (a != 'a') {

        a=Serial.read();

    }

}

void loop() {

    if (Serial.available()>0){ //checkk is any data has been sent by PC

        mode=Serial.read();

        switch (mode){

            case 'F': //Force sensor

                value=analogRead(A0); //sensor connected to A0

                Serial.println(value); //send value over serial

                break;

        }

    }

}

```

```
}
```

Force Sensitive Resister Sensor MATLAB Code

setupSerial.m

```
function [s,flag] = setupSerial(comPort)

%Initilize the serial port communication between Arduino and MATLAB

%Ensure that the arduino is also communicating with MATLAB at this time

flag=1;

s = serial(comPort);

set(s,'DataBits', 8 );

set(s,'StopBits', 1 );

set(s,'BaudRate', 9600);

set(s,'Parity)', 'none');

fopen(s);

a='b';

while (a~='a')

    a=fread(s,1,'uchar');

end

if (a=='a')
```

```

        disp('serial read');

end

fprintf(s,'%c','a');

mbox = msgbox('Serial Communicaiton setup. '); uiwait(mbox);

fscanf(s, '%u');

end

```

closeSerial.m

```

clear all

if ~isempty(instrfind)

    fclose(instrfind);

    delete(instrfind);

end

close all

disp('Serial Port Closed')

```

readFSR.m

```

function [force] = readFSR(out)

    fprintf(out,s,'F');

```



```

        force= fsanf(out.s,'%d');

end

fsr.m

clc;

close all;

clear all;

%% Sprecifies the COM port that the Arduino board is connected to

comPort = '/dev/tty.usbmodem1a12131';

if (~exist('serialFlag','var'))

    [fsr.s,serialFlag] = setupSerial(comPort);

end

%%italize the figure and buttons that will plot

if(~exist('h', 'var') || ~ishandle(h))

    h = figure(1);

end

if(~exist('text1', 'var'))

    text1 = uicontrol('Style', 'text','String', 'X:0 degrees',...

```

```

        'pos',[450 100 100 25], 'parent',h);

end

if(~exist('text2', 'var'))

    text1 = uicontrol('Style', 'text','String', 'Y:0 degrees',...

        'pos',[450 75 100 25], 'parent',h);

end

if(~exist('button', 'var'))

    text1 = uicontrol('Style', 'togglebutton','String', 'Stop & Close Serial Port',...

        'pos',[0 0 200 25], 'parent',h);

end

%Calibrate the sensor

weights=[0 20 50 70 100 120 150 200 250 500 750 1000];

m1=zeros(length(weights),1)';

%Read the values for each weight and assign it

for i=2:length(weights)

    mbox = msgbox(['Place' num2str(weights(i)) ' grams on the FSR']); uiwait(mbox);

    m1(i) = readFSR(fsr)

```

```

while (m1(i) < m1(i-1)) || m1(i) ==0;

    m1(i) = readFSR(fsr)

end

end

m=m1;

%%

% weights = [0 10 20 100 150 200 250 500 750 1000];

% m = [0 30 60 100 350 700 1800 4000 9000 29000 150000];

P1=polyfit( m, weights,2);

%Setup the graph

myaxes = axes('xlim',[-20 20],'ylim',[-20 20], 'zlim'...

    [0 250]);

view(3);

grid on;

axis equal;

hold on;

%Draw the 3d sphere

```

```

[xsphere ysphere zsphere] = sphere();

h(1) = surface(xsphere,ysphere,zsphere);

%Add the 3d sphere th figure

combinedobject = hgtransform('parent', myaxes);

set(h, 'parent', combinedobject)

drawnow

%%Acquire data and plot

while (get(button, 'Value') ==0)

    [voltage] = readFSR(fsr) %Read data from the FSR

    mass = polyval(P1, voltage) %In grams

    if (mass > 0

        force=mass*9.81; %In Newton

        %Update the readouts on the figure

        set(text1,'String', ['Mass : ' num2str(round(mass)) ' grams'])

        set(text2,'String', ['Force : ' num2str(round(mass)) ' N'])

        %Move sphere along z axis

        translation = makehgtform('translate',[0 0 mass];

```

```

set(combinedobject,'matrix',translation);

%Scale sphere to 1/10th of the mass

scaling = makehgtform('scale', mass/10;

set(combinedobject,'matrix',scaling);

%Set the translation and scaling to the sphere

set(combinedobject,'matrix',translation*scaling);

end

%Pause

pause(0.1);

end

%when graph closed close serial

closeSerial;

```